Chapter 12

Precise Analysis and Design of Multi-Layered Acoustic Wave Devices with Bragg Cell

Yongqiang Guo and Weiqiu Chen

Additional information is available at the end of the chapter

http://dx.doi.org/10.5772/54799

1. Introduction

The bulk acoustic wave (BAW) devices first emerged in 1920s and the surface acoustic wave (SAW) devices first appeared in 1960s (Royer & Dieulesaint, 2000). Since invented, these acoustic wave devices have been improved greatly in their performance and applications, along with significantly extended working parameters and application areas (Royer & Dieulesaint, 2000; Hashimoto, 2000). Nevertheless, in the last two decades, even more rigorous demands such as high operational frequency, high sensitivity, high reliability, multiple functionality, broad environment applicability, low attenuation and low cost, arise from the consumer, commercial and military applications. These demands challenge the conventional acoustic wave devices in which single crystalline piezoelectric materials are used as the wave medium. Therefore, the scheme of innovative acoustic wave devices utilizing piezoelectric multi-layered (stratified) structures was presented to cater for these demands. Fortunately, the successes of thin film deposition, etching and lithography technologies lead to the availability of piezoelectric multi-layered structures (Benetti et al., 2005). Recently, high-performance acoustic wave devices with multi-layered structures have been contrived and successfully fabricated (Kirsch et al., 2006; Benetti et al., 2008; Nakanishi et al., 2008; Brizoual et al., 2008). To further reduce the acoustic loss and enhance the quality factor of the multi-layered acoustic wave devices, Bragg Cell composed of many thin periodic alternate high- and low-impedance sublayers can be inserted between the propagation layer and the substrate. Efforts have been made on the fabrication of integrated piezoelectric multi-layered materials with Bragg Cell (Yoon & Park, 2000) and on the realization of superior multi-layered acoustic wave devices with Bragg Cell (Chung et al., 2008), especially aiming at the film bulk acoustic resonators (FBAR).

To ensure the well and stable performance of multi-layered acoustic wave devices, clear understanding of their operation status, especially the acoustic wave propagation behavior, is indispensable in the design process. Therefore, accurate and reliable modeling methods

are necessary. By far, three sorts of matrix methods, including the analytical methods based on continuous (distributed-parameter) models, numerical methods based on discrete models and analytical-numerical mixed methods, have been presented for analyzing multi-layered acoustic wave devices. Analytical matrix methods, such as the transfer matrix method (TMM) (Lowe, 1995; Adler, 2000), the effective permittivity matrix method (Wu & Chen, 2002), the scattering matrix method (Pastureaud et al., 2002), and the recursive asymptotic stiffness matrix method (Wang and Rokhlin, 2002), usually give accurate results with low computational cost. However, some of these analytical methods are numerically instable. One reason is that both exponentially growing and decaying terms with respect to frequency and thickness are incorporated in a same matrix, and the other is that matrix inversion is involved in the formulation. For example, TMM ceases to be effective for cases of high frequency-thickness products. Tan (2007) compared most analytical methods in their mathematical algorithm, computational efficiency and numerical stability. Very recently, Guo et al. (Guo, 2008; Guo & Chen, 2008a, 2010; Guo et al., 2009) have presented a new version of the analytical method of reverberation-ray matrix (MRRM) formerly proposed by Pao et al. (Su et al., 2002; Pao et al, 2007), based on three-dimensional elasticity/ piezoelectricity (Ding & Chen, 2001), state-space formalism (Stroh, 1962) and plane wave expansion for the analysis of free waves in multi-layered anisotropic structures. The new formulation of MRRM deals with the exponentially growing and decaying terms separately and refrains from matrix inversion. It is a promising analytical matrix method, which bearing unconditionally numerical stability, for accurately modeling the multi-layered acoustic wave devices (Guo and Chen, 2008b). Numerical methods, including the finite difference method (FDM), the finite element method (FEM), the boundary element method (BEM) and the hybrid method of BEM/FEM (Makkonen, 2005), are powerful for modeling multi-layered acoustic wave devices with complex geometries and boundaries. However, they are less accurate and efficient, especially for high frequency analysis. The reason is that the wave media should be modeled by tremendous elements of small size to ensure computational convergence. Analytical-numerical mixed methods, such as the finite element method/boundary integral formulation (FEM/BIF) (Ballandras et al., 2004) and the finite element method/spectral domain analysis (FEM/SDA) (Hashimoto et al., 2009; Naumenko, 2010), are usually powerful for modeling both the small-sized accessories and the large-dimensioned wave media with high accuracy. They seem to be promising as long as the uniformity of their formulation is improved (Hashimoto et al., 2009; Naumenko, 2010). Although some of these matrix methods are extendable to modeling the multi-layered acoustic wave devices with Bragg Cell, there are few investigations focused on this subject. Few studies have been reported on the effects of a Bragg Cell on wave propagation characteristics of multi-layered acoustic wave devices either. To the authors' knowledge, all existing references aimed at Bragg Cell in solidly mounted resonators. Zhang et al. (2006, 2008) and Marechal et al. (2008) studied both the resonant transmission in Bragg Cell and acoustic wave propagation in multi-layered bulk acoustic devices with Bragg Cell. Tajic et al., (2010) presented FEM combined with BEM and/or PML to simulate the solidly mounted BAW resonators with Bragg Cell. The formation mechanisms of the frequency bands in Bragg Cell are still an untouched topic. It should be pointed out that the Bragg Cell, as a kind of reliable wave guiding and isolating structure, is potential for utilizing in multi-layered

acoustic wave devices working with various acoustic modes including Rayleigh modes, Love modes, Lamb modes, SH modes and bulk longitudinal/transversal modes, so as to improve their performances (Yoon & Park, 2000; Chung et al., 2008). Moreover, for acoustic wave devices working with a specific acoustic mode, other spurious modes inevitably exist. Therefore, for appropriately designing the multi-layered acoustic wave devices with Bragg Cell, modeling methods should be established by considering various wave modes and based on an integrated model, which reckoning on the propagation media, electrodes, Bragg Cell, support layer and substrate. In addition, for appropriately designing the Bragg Cell to improve the performance of multi-layered acoustic wave devices, the features and the mechanisms of frequency bands in the Bragg Cell should be studied. The influence of inserted Bragg Cell on acoustic wave propagation in the working layer should also be clearly revealed.

In this chapter, the wave behavior in the Bragg Cell and the design rules of a Bragg Cell are studied by taking SH wave mode as illustration and by using the Method of Reverberation-Ray Matrix (MRRM). The MRRM is also proposed for accurate analysis and design of multi-layered acoustic wave devices with Bragg Cell, based on an integrated model involving the effects of electrodes, Bragg Cell, support layer and substrate on the working media. Firstly, the MRRM is extended to the analysis of SH wave dispersion characteristics of a ternary Bragg Cell, whose unit cell consisting of three isotropic layers. Based on the resultant closed-form dispersion equations, the formation mechanisms of the SH wave frequency bands are revealed. The design rules of the Bragg Cell according to specific isolation requirements of SH waves are summarized. Secondly, the integrated model, which incorporates the effects of electrodes, Bragg Cell, support layer and substrate on the working piezoelectric media by modeling them as individual non-piezoelectric or piezoelectric layers, is proposed for accurately analyzing acoustic wave propagation in multilayered acoustic wave devices. The formulation of MRRM for the integrated multi-layered structures based on the state space formalism is derived, by which the propagation characteristics of waves can be investigated. In view of the achieved dispersion characteristics, the operating status of various acoustic wave devices can be decided. Thirdly, numerical examples are given to validate the proposed MRRM, to show the features and the formation of SH-wave bands in the Bragg Cell and to indicate the resonant characteristics of multi-layered acoustic wave devices. Finally, conclusions are drawn concerning the SH wave behavior in the Bragg Cell, the advantages of the integrated model and MRRM, and the resonant characteristics of multi-layered acoustic wave devices.

2. The features and formation of SH-wave bands in the Bragg Cell

Consider an infinite periodic layered structure with each unit cell containing three isotropic elastic layers. A unit cell is depicted in Fig. 1, which can completely determine the band features of the infinite periodic layered structure by invoking the Floquet-Bloch principle (Mead, 1996). The surfaces and interfaces of the unit cell are denoted by numerals 1 to 4 from top to bottom, and the layers are represented by numerals 1 to 3 from top to bottom. Due to the isotropy of the layers, the in-plane wave motion is decoupled from the out-of-plane one. We limit our discussion to the out-of-plane (transverse) wave motion, i.e. only the SH type mode is present.

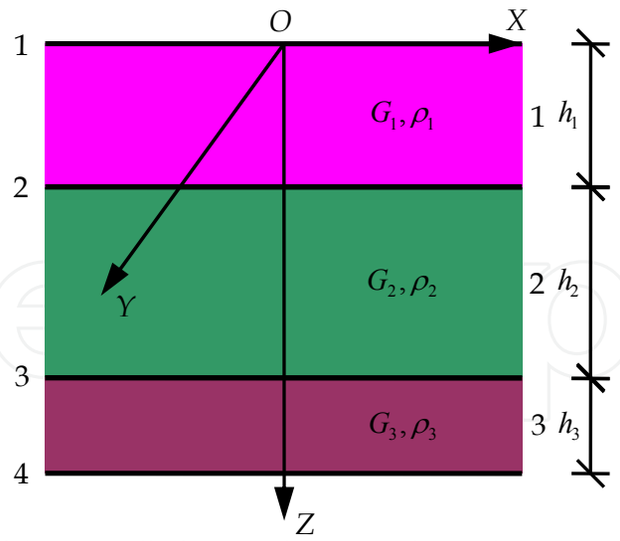

Figure 1. The schematic of the unit cell of a periodic ternary layered structure and its description in the global coordinates

2.1. SH wave dispersion characteristics of the Bragg Cell

Within the framework of the method of reverberation-ray matrix (MRRM) (Su et al., 2002; Pao et al., 2007; Guo, 2008), constituent layers of the unit cell are individually described in the corresponding local dual coordinates. Fig. 2 depicts the local dual coordinates of a typical layer j ($j=1,2,3$) with its top and bottom surfaces denoted respectively as J ($=j$) and K ($=j+1$), and the SH wave amplitudes along the thickness in the typical layer j as the wavenumber along X is k for all of the constituent layers. Meanwhile, superscripts *JK* or *KJ* will be attached to physical variables of the typical layer j, which is also called as JK or KJ according to the related coordinates (x^{JK}, y^{JK}, z^{JK}) or (x^{KJ}, y^{KJ}, z^{KJ}), to indicate the layer and its pertaining coordinate system. The displacement and stress are deemed to be positive as they are along the positive direction of the pertaining coordinates.

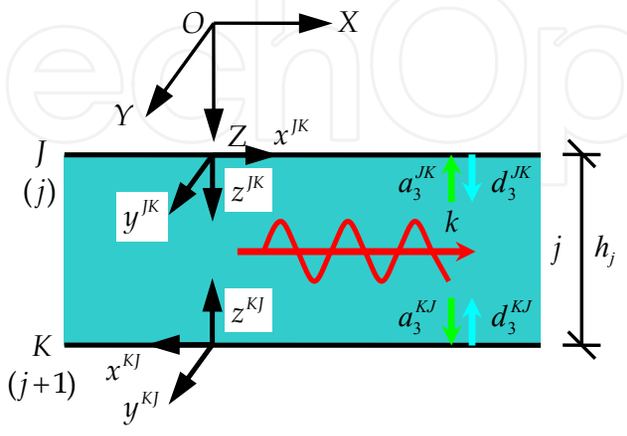

Figure 2. Description of a typical constituent layer j of the unit cell in local dual coordinates

According to the elastodynamics of linear isotropic media (Eringen & Suhubi, 1975), the plane wave solutions to the out-of-plane displacement v and shear stress τ_{zy} in any constituent layer *JK* (or *j*) in its pertaining coordinates (x^{JK}, y^{JK}, z^{JK}) can be expressed as follows (with superscripts *JK* omitted)

$$v(x,z,t) = \hat{v}(z)\mathrm{e}^{\mathrm{i}(\omega t - kx)} = (a_3\,\mathrm{e}^{\mathrm{i}\gamma_s z} + d_3\,\mathrm{e}^{-\mathrm{i}\gamma_s z})\mathrm{e}^{\mathrm{i}(\omega t - kx)}, \tag{1}$$

$$\tau_{zy}(x,z,t) = \hat{\tau}_{zy}(z)\mathrm{e}^{\mathrm{i}(\omega t - kx)} = \zeta_3(a_3\,\mathrm{e}^{\mathrm{i}\gamma_s z} - d_3\,\mathrm{e}^{-\mathrm{i}\gamma_s z})\mathrm{e}^{\mathrm{i}(\omega t - kx)}, \tag{2}$$

where $\hat{v}(z)$ and $\hat{\tau}_{zy}(z)$ signify the corresponding quantities in the frequency-wavenumber $(\omega - k)$ domain (i.e. the transformed quantities), $\mathrm{i} = \sqrt{-1}$ is the imaginary unit, γ_s $(= +\sqrt{k_s^2 - k^2}$ or $= -\sqrt{k_s^2 - k^2})$ and $k_s = \omega / c_s$ are respectively the z-direction shear wavenumber and the total shear wavenumber with ω being the circular frequency and $c_s = \sqrt{G/\rho}$ the shear wave velocity, $\zeta_3 = \mathrm{i}\gamma_s G$ is the shear stress coefficient, constants G and ρ are respectively the shear modulus and the mass density. It is clearly seen that the terms with a_3 and d_3 at the right-hand sides of Eqs. (1) and (2) signify backward and forward traveling waves along the thickness coordinate, i.e. the arriving and departing waves relative to the surface *J*, with a_3 and d_3 being the corresponding undetermined wave amplitudes.

First, we consider the spectral equations within the layers. The transformed displacement $\hat{v}$ (stress $\hat{\tau}_{zy}$) at an arbitrary plane z^{JK} of any layer j expressed in one coordinate system (x^{JK}, y^{JK}, z^{JK}) should be compatible with that expressed in the other coordinate system (x^{KJ}, y^{KJ}, z^{KJ}), due to the uniqueness of the physical essence. Referring to the sign convention of displacement (stress), we have

$$\hat{v}^{JK}(z^{JK}) = \hat{v}^{KJ}(h^{JK} - z^{JK}), \tag{3}$$

$$\hat{\tau}_{zy}^{JK}(z^{JK}) = -\hat{\tau}_{zy}^{KJ}(h^{JK} - z^{JK}). \tag{4}$$

Substituting Eq. (1) into Eq. (3) and Eq. (2) into Eq. (4), and noticing the functions $\mathrm{e}^{\mathrm{i}\gamma_s z}$ and $\mathrm{e}^{-\mathrm{i}\gamma_s z}$ are nonzero for finite γ_s and z, one obtains the phase relation of layer *j* (*JK* or *KJ*)

$$a_3^{KJ} = \mathrm{e}^{-\mathrm{i}\gamma_s^{JK} h^{JK}}\, d_3^{JK} = P_3^{KJ}(k,\omega) d_3^{JK} \tag{5}$$

where $\gamma_s^{JK} = \gamma_s^{KJ} = \gamma_{sj}$, $h^{JK} = h^{KJ} = h_j$ and $P_3^{JK} = P_3^{KJ} = P_{3j}$ are the wavenumber along z direction, the thickness and the phase coefficient of layer *j* (*JK* or *KJ*), respectively. It is noted that the thickness wavenumber γ_{sj} can always be chosen to satisfy $\mathrm{Re}[-\mathrm{i}\gamma_{sj} h_j] \le 0$, so that no exponentially growing function is included in the phase relation.

Second, we consider the spectral equations at the interfaces between adjacent layers. The compatibility of displacements and equilibrium of stresses at the interfaces 2 and 3 are expressed as

$$\hat{v}^{21}(0)=\hat{v}^{23}(0),\quad \hat{\tau}_{zy}^{21}(0)+\hat{\tau}_{zy}^{23}(0)=0,\quad \hat{v}^{32}(0)=\hat{v}^{34}(0),\quad \hat{\tau}_{zy}^{32}(0)+\hat{\tau}_{zy}^{34}(0)=0 \tag{6}$$

Substituting Eqs. (1) and (2) into Eq. (6), one obtains the scattering relations at interfaces 2 and 3

$$\begin{aligned} &a_3^{21}+d_3^{21}-a_3^{23}-d_3^{23}=0,\quad \zeta_3^{21}a_3^{21}-\zeta_3^{21}d_3^{21}+\zeta_3^{23}a_3^{23}-\zeta_3^{23}d_3^{23}=0\\ &a_3^{32}+d_3^{32}-a_3^{34}-d_3^{34}=0,\quad \zeta_3^{32}a_3^{32}-\zeta_3^{32}d_3^{32}+\zeta_3^{34}a_3^{34}-\zeta_3^{34}d_3^{34}=0 \end{aligned} \tag{7}$$

Third, we consider the spectral equations at the top and bottom surfaces. The Floquet-Bloch principle of periodic structures (Brillouin, 1953; Mead, 1996) requires that the displacement (stress) of bottom layer at the bottom surface 4 should relate to that of top layer at the top surface 1 by

$$\hat{v}^{43}(0)=\mathrm{e}^{\mathrm{i}qh}\,\hat{v}^{12}(0),\quad \hat{\tau}_{zy}^{43}(0)=-\mathrm{e}^{\mathrm{i}qh}\,\hat{\tau}_{zy}^{12}(0) \tag{8}$$

where $h=\sum_{j=1}^{3}h_j$ is the thickness of the unit cell, q is the wavenumber of the characteristic waves in the periodic ternary layered media. The real part $q_R h$ and the imaginary part $q_I h$ of dimensionless wavenumber qh denote the phase constant and the attenuation constant of the characteristic wave, respectively (Mead, 1996). Substitution of Eqs. (1) and (2) into Eq. (8) gives the scattering relations at surfaces 1 and 4

$$\mathrm{e}^{\mathrm{i}qh}a_3^{12}+\mathrm{e}^{\mathrm{i}qh}d_3^{12}-a_3^{43}-d_3^{43}=0,\quad \mathrm{e}^{\mathrm{i}qh}\zeta_3^{12}a_3^{12}-\mathrm{e}^{\mathrm{i}qh}\zeta_3^{12}d_3^{12}+\zeta_3^{43}a_3^{43}-\zeta_3^{43}d_3^{43}=0 \tag{9}$$

Finally, introducing the phase relations of all layers as given in Eq. (5) to the scattering relations of all interfaces and surfaces as given in Eqs. (7) and (9), we obtain the system equations with all the departing wave amplitudes as basic unknown quantities

$$\begin{bmatrix} P_3^{21} & 1 & -1 & -P_3^{23} & 0 & 0\\ \zeta_3^{21}P_3^{21} & -\zeta_3^{21} & -\zeta_3^{23} & \zeta_3^{23}P_3^{23} & 0 & 0\\ 0 & 0 & P_3^{32} & 1 & -1 & -P_3^{34}\\ 0 & 0 & \zeta_3^{32}P_3^{32} & -\zeta_3^{32} & -\zeta_3^{34} & \zeta_3^{34}P_3^{34}\\ \mathrm{e}^{\mathrm{i}qh} & \mathrm{e}^{\mathrm{i}qh}P_3^{12} & 0 & 0 & -P_3^{43} & -1\\ -\zeta_3^{12}\mathrm{e}^{\mathrm{i}qh} & \zeta_3^{12}\mathrm{e}^{\mathrm{i}qh}P_3^{12} & 0 & 0 & \zeta_3^{43}P_3^{43} & -\zeta_3^{43} \end{bmatrix} \begin{Bmatrix} d_3^{12}\\ d_3^{21}\\ d_3^{23}\\ d_3^{32}\\ d_3^{34}\\ d_3^{43} \end{Bmatrix} = \begin{Bmatrix} 0\\0\\0\\0\\0\\0 \end{Bmatrix}$$

or

$$\mathbf{R}_d(k,\omega,q)\mathbf{d}=\mathbf{0} \tag{10}$$

where $\zeta_3^{JK}=\zeta_3^{KJ}=\zeta_{3j}$ ($J=K-1=j=1,2,3$) is the shear stress coefficient of layer j, $\mathbf{R}_d$ is the system matrix, and $\mathbf{d}$ is the global departing wave vector.

The dispersion equation governing the characteristic SH waves in periodic ternary layered media is obtained by vanishing of the determinant of system matrix

$$\det[\mathbf{R}_d(k,\omega,q)] = \mathbf{0}. \tag{11}$$

Further expansion of the determinant in Eq. (11) gives the closed-form dispersion relation of characteristic SH waves in periodic ternary layered media as follows

$$\begin{aligned}
&8\zeta_{31}\zeta_{32}\zeta_{33}\,\mathrm{e}^{-\mathrm{i}\gamma_{s1}h_1}\,\mathrm{e}^{-\mathrm{i}\gamma_{s2}h_2}\,\mathrm{e}^{-\mathrm{i}\gamma_{s3}h_3}(1+\mathrm{e}^{2\mathrm{i}qh})\\
&-2\zeta_{31}\zeta_{32}\zeta_{33}\,\mathrm{e}^{\mathrm{i}qh}(1+\mathrm{e}^{-2\mathrm{i}\gamma_{s1}h_1})(1+\mathrm{e}^{-2\mathrm{i}\gamma_{s2}h_2})(1+\mathrm{e}^{-2\mathrm{i}\gamma_{s3}h_3})\\
&-\left[(\zeta_{31})^2+(\zeta_{32})^2\right]\zeta_{33}\,\mathrm{e}^{\mathrm{i}qh}(1-\mathrm{e}^{-2\mathrm{i}\gamma_{s1}h_1})(1-\mathrm{e}^{-2\mathrm{i}\gamma_{s2}h_2})(1+\mathrm{e}^{-2\mathrm{i}\gamma_{s3}h_3})\\
&-\left[(\zeta_{32})^2+(\zeta_{33})^2\right]\zeta_{31}\,\mathrm{e}^{\mathrm{i}qh}(1-\mathrm{e}^{-2\mathrm{i}\gamma_{s2}h_2})(1-\mathrm{e}^{-2\mathrm{i}\gamma_{s3}h_3})(1+\mathrm{e}^{-2\mathrm{i}\gamma_{s1}h_1})\\
&-\left[(\zeta_{33})^2+(\zeta_{31})^2\right]\zeta_{32}\,\mathrm{e}^{\mathrm{i}qh}(1-\mathrm{e}^{-2\mathrm{i}\gamma_{s3}h_3})(1-\mathrm{e}^{-2\mathrm{i}\gamma_{s1}h_1})(1+\mathrm{e}^{-2\mathrm{i}\gamma_{s2}h_2}) = 0.
\end{aligned} \tag{12}$$

Dispersion equation (12) assures unconditionally numerical stability because $\mathrm{Re}[-\mathrm{i}\gamma_{sj}h_j] \le 0$ is already guaranteed by the properly established phase relation and $\mathrm{Re}[\mathrm{i}qh] \le 0$ can also be guaranteed by properly specifying q in the solving process, since $+q$ and $-q$ signifying wavenumbers in opposite direction should give the same propagation characteristics. Due to $\mathrm{e}^{-\mathrm{i}\gamma_{sj}h_j} \neq 0$ and $\mathrm{e}^{\mathrm{i}qh} \neq 0$, Equation (12) can be simplified, by virtue of relations between trigonometric functions and exponential functions, to

$$\begin{aligned}
&2\zeta_{31}\zeta_{32}\zeta_{33}\left[\cos(qh)-\cos(\gamma_{s1}h_1)\cos(\gamma_{s2}h_2)\cos(\gamma_{s3}h_3)\right] =\\
&-\left[(\zeta_{31})^2+(\zeta_{32})^2\right]\zeta_{33}\sin(\gamma_{s1}h_1)\sin(\gamma_{s2}h_2)\cos(\gamma_{s3}h_3)\\
&-\left[(\zeta_{32})^2+(\zeta_{33})^2\right]\zeta_{31}\sin(\gamma_{s2}h_2)\sin(\gamma_{s3}h_3)\cos(\gamma_{s1}h_1)\\
&-\left[(\zeta_{33})^2+(\zeta_{31})^2\right]\zeta_{32}\sin(\gamma_{s3}h_3)\sin(\gamma_{s1}h_1)\cos(\gamma_{s2}h_2).
\end{aligned} \tag{13}$$

Define

$$Z_{SHj} = \zeta_{3j}/\mathrm{i}\omega = \gamma_{sj}G_j/\omega = \sqrt{\rho_j G_j - k^2 G_j^2/\omega^2} \tag{14}$$

as the characteristic impedance of SH wave in layer j, which is dependent on not only the shear modulus G_j and mass density ρ_j, but also the frequency ω and wavenumber k. Therefore, the characteristic impedance of SH wave in an isotropic layer is not a constant and can be imaginary below the cutoff frequency of SH wave. It is very different from the characteristic impedance of bulk shear wave $Z_{Tj} = \sqrt{\rho_j G_j}$ in an isotropic medium j, which is a real-valued constant. But Z_{SHj} equals to Z_{Tj} as $k = 0$. If $Z_{SH1}Z_{SH2}Z_{SH3} = 0$, i.e. $(\omega \pm kc_{s1})(\omega \pm kc_{s2})(\omega \pm kc_{s3}) = 0$, the dispersion equation (13) is automatically satisfied regardless of qh. This case merely gives the cutoff frequency of SH wave mode $\omega_c = |k|c_s$

within one of the constituent layers, and we shall not discuss it any further. Otherwise for $Z_{SH1}Z_{SH2}Z_{SH3} \neq 0$, the dispersion relation is further simplified to

$$\begin{aligned}\cos(qh) &= \cos(\gamma_{s1}h_1)\cos(\gamma_{s2}h_2)\cos(\gamma_{s3}h_3) - \frac{1}{2}(F_{1/2}+F_{2/1})\sin(\gamma_{s1}h_1)\sin(\gamma_{s2}h_2)\cos(\gamma_{s3}h_3) \\ &-\frac{1}{2}(F_{2/3}+F_{3/2})\sin(\gamma_{s2}h_2)\sin(\gamma_{s3}h_3)\cos(\gamma_{s1}h_1) - \frac{1}{2}(F_{3/1}+F_{1/3})\sin(\gamma_{s3}h_3)\sin(\gamma_{s1}h_1)\cos(\gamma_{s2}h_2),\end{aligned} \tag{15}$$

where

$$F_{j'/j''} = \frac{\zeta_{3j'}}{\zeta_{3j''}} = \frac{\mathrm{i}\gamma_{sj'}G_{j'}}{\mathrm{i}\gamma_{sj''}G_{j''}} = \frac{\gamma_{sj'}G_{j'}/\omega}{\gamma_{sj''}G_{j''}/\omega} = \frac{Z_{SHj'}}{Z_{SHj''}} \quad \left(j', j'' = 1,2,3, j' \neq j''\right) \tag{16}$$

signifies the contrast of characteristic impedances of SH waves in layer j' and layer j''.

2.2. Formation mechanisms of SH-wave bands in the Bragg Cell

Based on Eq. (15), in which $Z_{SH1}Z_{SH2}Z_{SH3} \neq 0$ is implied, in what follows we will discuss the formation mechanisms of frequency bands of SH waves in periodic ternary layered media, according to the following two cases for the characteristic impedances of SH waves in the three constituent layers of the unit cell.

1. $Z_{SH1} = Z_{SH2} = Z_{SH3}$

Owing to $F_{j'/j''} = F_{j''/j'} = 1$ ($j', j'' = 1,2,3$, $j' \neq j''$), the dispersion relation (15) is reduced to

$$\begin{aligned}\cos(qh) &= \cos(\gamma_{s1}h_1 + \gamma_{s2}h_2 + \gamma_{s3}h_3) = \cos(\gamma_{se}h) \\ &= \cos\left(\frac{\omega}{c_{SH1}}h_1 + \frac{\omega}{c_{SH2}}h_2 + \frac{\omega}{c_{SH3}}h_3\right) = \cos[\omega(T_{SH1}+T_{SH2}+T_{SH3})] = \cos(\omega T_{SH}),\end{aligned} \tag{17}$$

where $\gamma_{se} = \sum_{j=1}^{3}(\gamma_{sj}h_j)/h$ is the equivalent wavenumber of SH wave in the unit cell, $T_{SHj} = h_j / c_{SHj}$ is the parameter reflecting the characteristic time as SH wave traverses the thickness of constituent *j*, but may be imaginary number below the cutoff frequency ω_c, $T_{SH} = \sum_{j=1}^{3} T_{SHj}$ is the parameter reflecting the characteristic time as SH wave traverses the thickness of the unit cell. Equation (17) has the solution

$$qh = \pm\gamma_{se}h + 2\frac{m}{n}\pi = \pm\omega T_{SH} + 2\frac{m}{n}\pi, \tag{18}$$

where m and n are arbitrary integers corresponding to positive and negative signs, respectively . Equation (18) indicates that when all the three constituent layers have the same characteristic impedance of SH wave, there is no bandgap above the maximum cutoff frequency $\omega_{c\max} = \max(\omega_{c1}, \omega_{c2}, \omega_{c3})$. The dispersion spectra are completely determined by

the fundamental dispersion curve of the equivalent SH wave in the unit cell due to the zone folding effect (Brillouin, 1953) with the characteristic time of the unit cell being the essential parameter. In other words, the contrast of characteristic impedances determines whether the band gaps exist or not above $\omega_{c\max}$, and the characteristic time of the unit cell decides the dispersion spectra of the periodic layered media as no bandgap exists above $\omega_{c\max}$.

2. $Z_{SHj} \neq Z_{SHj'}, Z_{SHj} \neq Z_{SHj''}$ ($Z_{SHj'} = or \neq Z_{SHj''}$, $j, j', j'' = 1$ or 2 or 3 , $j \neq j' \neq j''$)

If $Z_{SHj'} = Z_{SHj''}$, then the dispersion relation (15) is reduced to

$$\begin{aligned}\cos(qh) &= \cos(\gamma_{sj}h_j)\cos(\gamma_{sj'}h_{j'} + \gamma_{sj''}h_{j''}) - \frac{1}{2}(F_{j/j'} + F_{j'/j})\sin(\gamma_{sj}h_j)\sin(\gamma_{sj'}h_{j'} + \gamma_{sj''}h_{j''}) \\ &= \cos(\gamma_{sj}h_j)\cos(\gamma_{si}h_i) - \frac{1}{2}(F_{j/i} + F_{i/j})\sin(\gamma_{sj}h_j)\sin(\gamma_{si}h_i),\end{aligned} \tag{19}$$

which is the dispersion relation for periodic binary layered media already obtained (Shen & Cao, 2000; Wang et al., 2004). $\gamma_{si} = (\gamma_{sj'}h_{j'} + \gamma_{sj''}h_{j''})/h_i$ and $h_i = h_{j'} + h_{j''}$ are the wavenumber along the z-direction and the thickness of the new equivalent layer i composed of the two constituent layers with identical characteristic impedance of SH wave. If $Z_{SHj'} \neq Z_{SHj''}$, then the dispersion relation should be the general form of Eq. (15).

In any circumstances, as $\omega > \omega_{c\max}$ the characteristic impedances and the wavenumbers along the z-direction of SH waves in the constituent layers will be positive real number. Thus, we have

$$F_{j/\Gamma} + F_{\Gamma/j} = 1 - \varepsilon_{j/\Gamma} + \frac{1}{1-\varepsilon_{j/\Gamma}} = \frac{1}{1-\varepsilon_{\Gamma/j}} + 1 - \varepsilon_{\Gamma/j} = 1 - \varepsilon_{j\Gamma} + \frac{1}{1-\varepsilon_{j\Gamma}} = 2 + \sum_{b=2}^{+\infty}\varepsilon_{j\Gamma}^{b} \quad (\Gamma = j', j'') \tag{20}$$

where $\varepsilon_{j/\Gamma}$, $\varepsilon_{\Gamma/j}$ and $\varepsilon_{j\Gamma}$ are real numbers, $0 < \varepsilon_{j/\Gamma} < 1$ ($\varepsilon_{\Gamma/j} > 1$) when $F_{j/\Gamma} < 1$, $0 < \varepsilon_{\Gamma/j} < 1$ ($\varepsilon_{j/\Gamma} > 1$) when $F_{\Gamma/j} < 1$, $\varepsilon_{j\Gamma} = \min(\varepsilon_{j/\Gamma}, \varepsilon_{\Gamma/j}) \in (0,1)$. Similarly, we have

$$F_{j'/j''} + F_{j''/j'} = 1 - \varepsilon_{j'j''} + \frac{1}{1-\varepsilon_{j'j''}} = 2 + \sum_{b=2}^{+\infty}\varepsilon_{j'j''}^{b}, \tag{21}$$

where $\varepsilon_{j'j''} = 0$ as $Z_{SHj'} = Z_{SHj''}$, $0 < \varepsilon_{j'j''} < 1$ as $Z_{SHj'} \neq Z_{SHj''}$. Therefore, the dispersion equations (15) and (19) can be rewritten uniformly as

$$
\begin{aligned}
&\cos(qh)=\cos(\gamma_{se}h)-\frac{1}{2}\sum_{b=2}^{+\infty}\varepsilon_{jj'}^{b}\sin(\gamma_{sj}h_j)\sin(\gamma_{sj'}h_{j'})\cos(\gamma_{sj''}h_{j''})\\
&-\frac{1}{2}\sum_{b=2}^{+\infty}\varepsilon_{jj''}^{b}\sin(\gamma_{sj}h_j)\sin(\gamma_{sj''}h_{j''})\cos(\gamma_{sj'}h_{j'})-\frac{1}{2}\sum_{b=2}^{+\infty}\varepsilon_{j'j''}^{b}\sin(\gamma_{sj'}h_{j'})\sin(\gamma_{sj''}h_{j''})\cos(\gamma_{sj}h_j)\\
&=\cos(\gamma_{se}h)-\frac{\varepsilon_{jj'}^{2}}{2(1-\varepsilon_{jj'})}\sin(\gamma_{sj}h_j)\sin(\gamma_{sj'}h_{j'})\cos(\gamma_{sj''}h_{j''})\\
&-\frac{\varepsilon_{jj''}^{2}}{2(1-\varepsilon_{jj''})}\sin(\gamma_{sj}h_j)\sin(\gamma_{sj''}h_{j''})\cos(\gamma_{sj'}h_{j'})-\frac{\varepsilon_{j'j''}^{2}}{2(1-\varepsilon_{j'j''})}\sin(\gamma_{sj'}h_{j'})\sin(\gamma_{sj''}h_{j''})\cos(\gamma_{sj}h_j)\\
&=\cos(\omega T_{SH})-\frac{\varepsilon_{jj'}^{2}}{2(1-\varepsilon_{jj'})}\sin(\omega T_{SHj})\sin(\omega T_{SHj'})\cos(\omega T_{SHj''})\\
&-\frac{\varepsilon_{jj''}^{2}}{2(1-\varepsilon_{jj''})}\sin(\omega T_{SHj})\sin(\omega T_{SHj''})\cos(\omega T_{SHj'})-\frac{\varepsilon_{j'j''}^{2}}{2(1-\varepsilon_{j'j''})}\sin(\omega T_{SHj'})\sin(\omega T_{SHj''})\cos(\omega T_{SHj}),
\end{aligned}
\tag{22}
$$

which indicates that the band structures of the periodic ternary layered media are not only determined by the fundamental dispersion curve of the equivalent SH wave according to zone folding effect, but also influenced by three disturbance terms with disturbing functions $\sin(\gamma_{sj'}h_{j'})\sin(\gamma_{sj''}h_{j''})\cos(\gamma_{sj}h_j)$ (or $\sin(\omega T_{SHj'})\sin(\omega T_{SHj''})\cos(\omega T_{SHj})$, $j,j',j''=1,2,3$, $j\neq j'\neq j''$) and disturbing amplitudes $\varepsilon_{j'j''}^{2}/[2(1-\varepsilon_{j'j''})]$. The value of the right-hand side of Eq. (22) determines the demarcation of frequency bands: ±1 gives the dividing lines of pass-bands and stop-bands; 0 gives the central frequencies of pass-bands; those between -1 and 1 give the pass-bands; and all other values give the stop-bands. The characteristic time of the unit cell, the characteristic times of constituent layers and the contrasts of characteristic impedances of SH waves in the constituent layers are the essential parameters for the band structure formation, which determine the shape of the dispersion curves of the equivalent SH wave (the pre-disturbed baselines), the shapes of the disturbing functions, and the amplitudes of the disturbance terms, respectively. When the disturbing functions satisfy $\sin(\gamma_{sj'}h_{j'})\sin(\gamma_{sj''}h_{j''})\cos(\gamma_{sj}h_j)=0$ ($\sin(\gamma_{sj'}h_{j'})\sin(\gamma_{sj''}h_{j''})\cos(\gamma_{sj}h_j)=\pm1$), the band structures coincide exactly with (deviate most from) the fundamental and derivative dispersion curves of the equivalent SH wave in the unit cell. The corresponding points on the dispersion curves are called as the coincident (separating) points. The frequency equation can be simplified to ($j,j',j''=1,2,3$, $j\neq j'\neq j''$)

$$
\begin{aligned}
&\gamma_{sj'}h_{j'}=g_{j'}\pi,\ \gamma_{sj''}h_{j''}=g_{j''}\pi\ \left(g_{j'}\text{ and }g_{j''}\text{ are integers}\right)\text{or}\\
&\gamma_{sj}h_j=(2g_j+1)\pi/2,\ \gamma_{sj'}h_{j'}=(2g_{j'}+1)\pi/2,\ \gamma_{sj''}h_{j''}=(2g_{j''}+1)\pi/2
\end{aligned}
\tag{23}
$$

$$
\gamma_{sj}h_j=g_j\pi,\ \gamma_{sj'}h_{j'}=(2g_{j'}+1)\pi/2,\ \gamma_{sj''}h_{j''}=(2g_{j''}+1)\pi/2,
\tag{24}
$$

for coincident and separating points, respectively.

In physics, at any interface J of the unit cell there are one incident wave w_{ij} and one reflected wave w_{rj} arising from the next interface except that there is no reflection at the interface where the two constituent layers with identical characteristic impedances connected. $\gamma_{sj}h_j$, $\gamma_{sj'}h_{j'}$ and $\gamma_{sj''}h_{j''}$ denote the phase changes as SH wave passes through layer j, j' and j'', respectively. Thus, the former formula in Eq. (23) corresponds to the constructive interference condition of the incident wave and reflected wave at two interfaces, and the latter formula in Eq. (23) corresponds to the destructive interference condition at three interfaces. Equation (24) corresponds to destructive interference condition of incident wave and reflected wave at two interfaces and constructive interference condition at one interface. Therefore, it is concluded that the frequency bands are formed physically as a result of interference phenomenon as waves transmit and reflect in the constituent layers of a periodic ternary layered media. The specified combination of exact constructive and destructive interferences of the incident and reflected waves at some interfaces makes the equivalent SH wave travel through the unit cell without any change of its dispersion characteristic or be completely prohibited to travel. The specified combination of near constructive and destructive interferences of the incident and reflected waves at some interfaces makes the equivalent SH wave be capable of going through the unit cell with a change of its dispersion characteristic or be attenuated. The exact constructive and destructive interferences specified by Eq. (23) and Eq. (24) are only possible for special periodic ternary layered media with the characteristic times of constituent layers satisfying

$$T_{SHj'} : T_{SHj''} = g_{j'} : g_{j''} \quad \text{or} \quad T_{SHj} : T_{SHj'} : T_{SHj''} = (2g_j + 1) : (2g_{j'} + 1) : (2g_{j''} + 1) \tag{25}$$

$$T_{SHj} : T_{SHj'} : T_{SHj''} = g_j : (2g_{j'} + 1) : (2g_{j''} + 1) \tag{26}$$

However, the near constructive and destructive interferences specified by Eq. (23) and Eq. (24) can occur in general periodic ternary layered media.

In summary, the occurrence of some specified combination of exact or near constructive and destructive interference phenomena in the unit cell makes the equivalent SH wave travel through the unit cell and gives birth to the pass-bands, whereas the occurrence of other specified combination of exact or near destructive interference makes the equivalent SH wave unable to pass through the unit cell and brings about the stop-bands. Although the above discussion on the formation mechanisms of SH-wave bands is based on the periodic ternary layered structure, it is actually extendable to SH wave in general periodic layered media.

2.3. Design rules to the Bragg Cell concerning with SH wave bands

The discussion of formation mechanisms of SH wave bands in the layered Bragg Cell indicates that the contrasts of characteristic impedances of the constituent layers, the characteristic time of the unit cell and the characteristic times of the constituent layers are three kinds of essential parameters, which influence the band properties. First, the contrasts of characteristic impedances decide whether the stop-bands other than that due to SH wave

cutoff property exist or not. When the characteristic impedances of all the constituent layers are identical, any SH waves above the maximum cutoff frequency can propagate in the periodic layer without attenuation and no stop-bands other than that due to the SH wave cutoff property exist. In other cases, stop-bands exist above the maximum cutoff frequency, and the contrasts of characteristic impedances decide the widths of the frequency bands. The characteristic time of the unit cell decides the slopes of the dispersion curves of equivalent SH waves, thus it definitely specifies the number of pass-bands/stop-bands in a given frequency range. The characteristic times of the constituent layers mainly decide the mid-frequencies of the frequency bands. It should be pointed out that the mass densities and shear moduli of constituent layers affect all the three kinds of essential parameters, while the thicknesses of the constituent layers only influence the characteristic times of the unit cell and of the constituent layers. These rules can be used for the design of layered Bragg Cells according to the SH-wave bands requirements.

2.4. Numerical examples

In this section, the above proposed MRRM for dispersion characteristic analysis and the mechanisms for band structure formation of SH waves in periodic ternary layered media are validated by considering a periodic ternary layered structure with the unit cell consisting of one Pb layer in the middle and two epoxy layers at the up and down sides. The thickness of the Pb layer is 10mm and that of the epoxy layers is 5mm. The material parameters of Pb and epoxy including the Young's modulus, shear modulus and mass density are $E_{Pb} = 40.8187$ GPa, $E_{epoxy} = 4.35005$ GPa, $G_{Pb} = 14.9$ GPa, $G_{epoxy} = 1.59$ GPa, $\rho_{Pb} = 11600$ kg/m^3 and $\rho_{epoxy} = 1180$ kg/m^3. The band structures of SH waves in this periodic ternary layered medium are calculated by the formulation presented in Section 2.1. For the convenience of presentation, the results are represented by the dimensionless wavenumbers kh/π and qh/π with $h = 0.02$ m being the total thickness of the unit cell, and the engineering frequency $f = \omega/2\pi$.

We first consider the property of SH-wave band structures in the exemplified periodic ternary layered medium. Figure 3 gives the band structures of SH waves below 140 kHz represented as various forms of graphs. Figure 3(a) depicts the phase constant surfaces in the pass-bands as the dimensionless wavenumbers kh/π and qh/π are in the range of $[-2,2]$. Figures 3(b) to 3(d) describe both the phase constant spectra in pass-bands (i.e. the relation between f and $q_R h/\pi$) and the attenuation constant spectra in stop-bands (i.e. the relation between f and $q_I h/\pi$) as the dimensionless wavenumber kh/π is 1.0, 0.5 and 0.0, respectively. Figure 3(e) plots the relation between f and $|k|h/\pi$ when qh/π is specified as $0.0+2I_1$, $0.5+2I_2$ and $1.0+2I_3$ with I_1, I_2 and I_3 being arbitrary integers. To validate our obtained results, in Fig. (3d) the phase constant spectra as $kh/\pi = 0$ are compared to the corresponding results calculated by Wang et al. (2004), and in Fig. (3e) the spectra of f versus $|k|h/\pi$ as $qh/\pi = 0+2I_1$ and $qh/\pi = 1+2I_3$ are compared to their counterparts calculated by Wang et al. (2004).

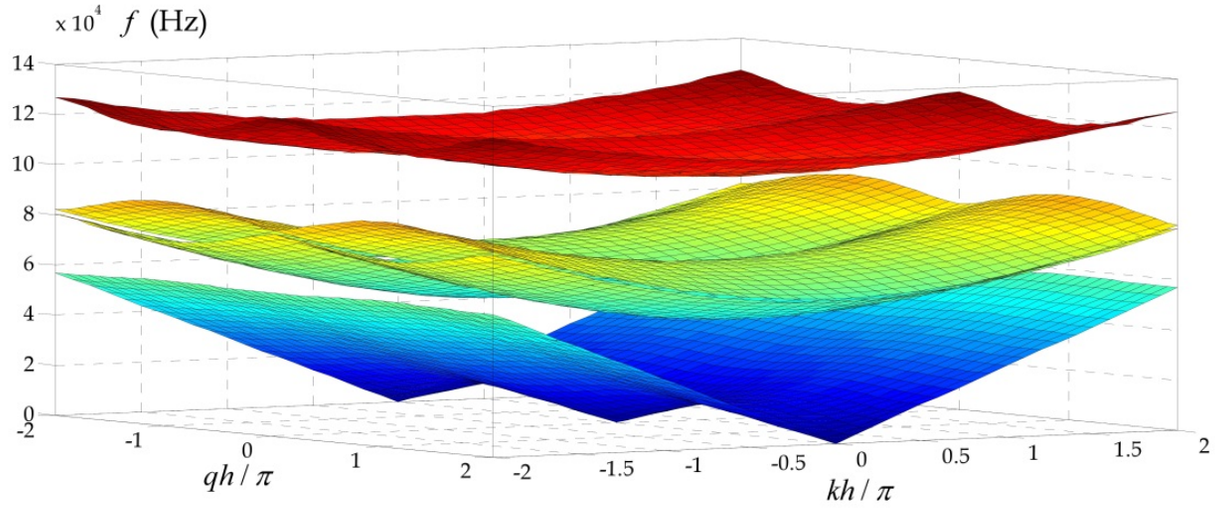

(a) The phase constant surfaces in the pass-bands

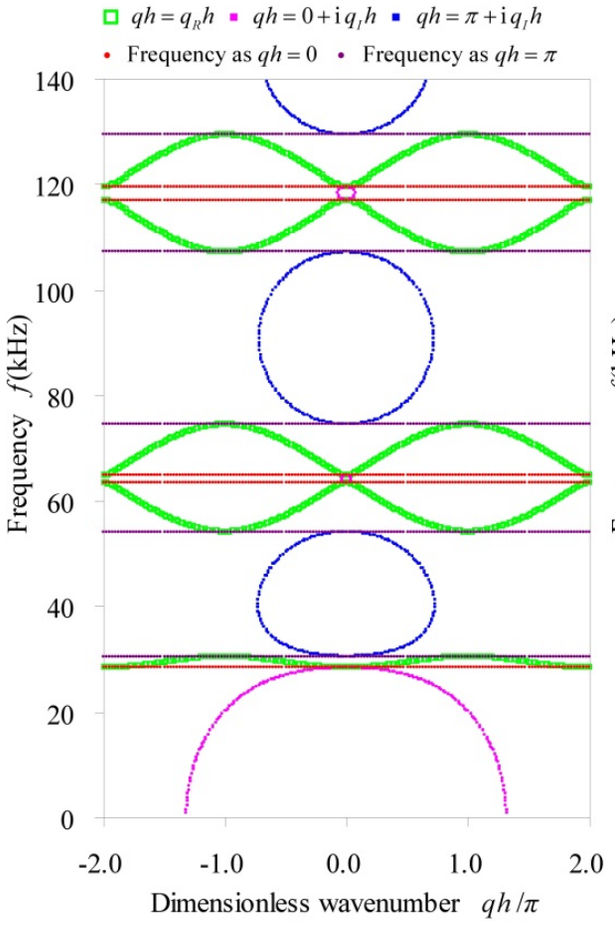

(b) The band structures as kh/π=1.0

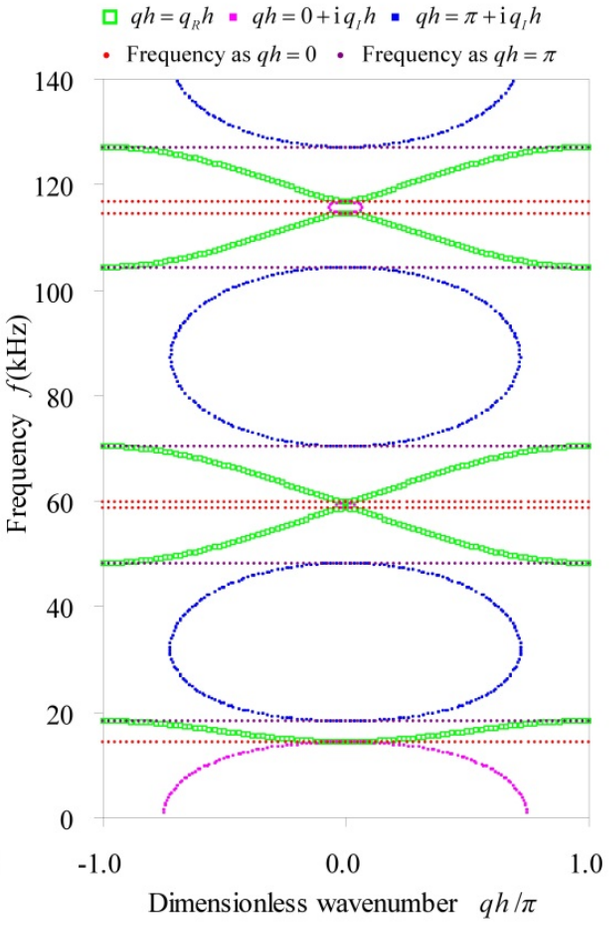

(c) The band structures as kh/π=0.5

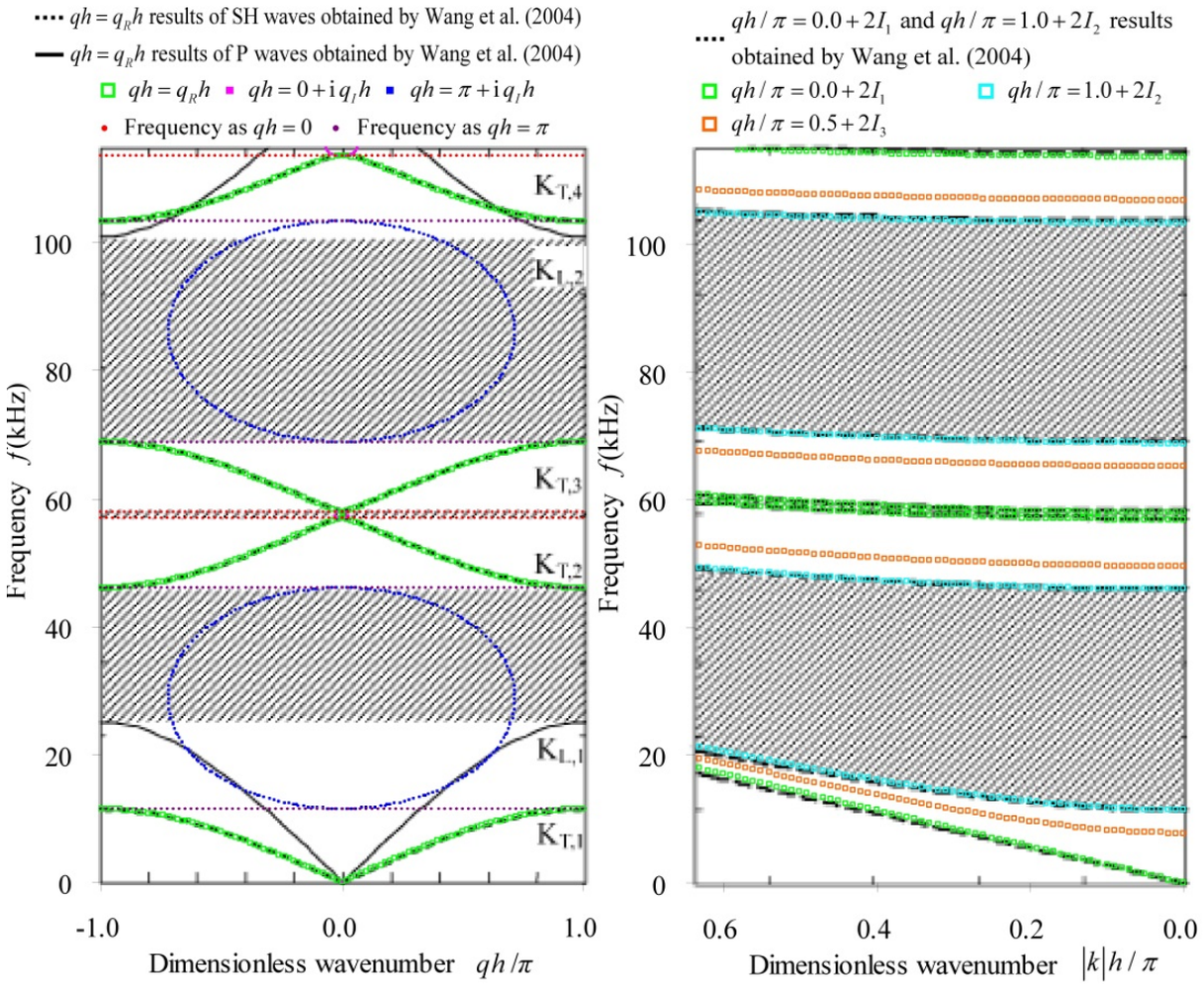

(d) The band structures as kh/π=0.0

(e) The relation between f and kh/π when qh/π are specified as 0.0+2I_1, 0.5+2I_2 and 1.0+2I_3

Figure 3. The band structures of SH waves below 140 kHz in the periodic ternary layered medium consisting of one Pb layer and two epoxy layers

It is seen from Fig. 3(a) that the phase constant surfaces in the pass-bands are symmetrical with respect to the vertical plane $kh/\pi = 0$, which indicates that the SH waves along the positive and the negative X directions have identical propagation properties. This is due to the symmetry of structural configuration and material parameters of the exemplified periodic ternary layered medium with respect to YOZ plane. Likewise, the phase constant surfaces in Fig. 3(a) and the attenuation constant spectra in Figs. 3(b) to 3(d) are also symmetry with respect to $qh/\pi = 0$, which indicates that the upward and downward characteristic SH waves have identical band structures. In addition, the phase constant surfaces in Fig. 3(a) are periodical with respect to qh/π as the minimum positive period being $qh/\pi = 2$, which indicates the periodicity of propagating characteristic SH waves along the thickness of the unit cell and reflects the zone folding effect of periodic structures.

Figs. 3(b) to 3(d) signify that for any kh/π, with the increasing of frequency the phase constant spectra and the attenuation constant spectra of characteristic SH waves in periodic ternary layered media occur alternately, i.e. the pass-bands and the stop-bands occur alternately. However, the attenuation spectra (the stop band) will advent first for any kh/π except for $kh/\pi = 0$. It should be noted that as $kh/\pi \neq 0$, the first stop band is formed due to the cutoff property of the SH waves in the constituent layers. For any kh/π, the attenuation constant spectra in form of closed loops with phase 0 and phase π appear alternately. It indicates from Figs. 3(b) to 3(e) that for any kh/π, the frequencies as $qh/\pi = 0$ and those as $qh/\pi = 1$, which are respectively identical to those as $qh/\pi = 0 + 2I_1$ and those as $qh/\pi = 1 + 2I_3$, are the demarcations between the pass-bands and the stop-bands. The ranges between two adjacent bounding frequencies, with one corresponding to $qh/\pi = 0 + 2I_1$ and the other corresponding to $qh/\pi = 1 + 2I_3$ are pass-bands, whereas the ranges between two adjacent bounding frequencies with both corresponding to $qh/\pi = 0 + 2I_1$ or $qh/\pi = 1 + 2I_3$ are stop-bands. Fig. 3(e) shows the f - $|k|h/\pi$ spectra as qh/π takes any other real value lie in the pass-bands between the f - $|k|h/\pi$ spectra as $qh/\pi = 0$ and those as $qh/\pi = 1$. With the increasing of $|k|h/\pi$, the demarcating frequencies of the corresponding frequency-bands rise. The first demarcation frequency increases most obviously with the rise of $|k|h/\pi$.

In Fig. 3(d), the comparison between the phase constant spectra obtained by our proposed method and those calculated by Wang et al. (2004) indicates good agreement. In Fig. 3(e), the comparison between the f - $|k|h/\pi$ spectra obtained by our method and those calculated by Wang et al. (2004) also manifests close coincidence. Furthermore, the f - $|k|h/\pi$ spectra corresponding to $qh/\pi = 0 + 2I_1$ and $qh/\pi = 1 + 2I_3$ in our results are explicitly separated, which clearly denotes the pass-bands and stop-bands. All these validate the accuracy and excellence of the proposed MRRM for dispersion characteristic analysis.

Let us now consider the formation of SH-wave band structures in the exemplified periodic ternary layered structure. We plot in Figs. (4a) and (4b) the phase and the attenuation constant spectra of characteristic SH waves together with the dispersion curves of the equivalent SH waves in the exemplified periodic ternary layered structure, as $kh/\pi = 0.0$ and $kh/\pi = 0.5$, respectively, for illustrating the close relation between the dispersion curves of the equivalent SH waves and the band structures of characteristic SH waves. The fundamental real-part and the imaginary-part dispersion curves of the equivalent SH waves are obtained directly from the definition $\gamma_{se}h = \sum_{j=1}^{3} h_j \sqrt{\omega^2 / c_{sj}^2 - k^2}$, while the derivative real-part dispersion curve of the equivalent SH waves are attained by virtue of the zone folding effect.

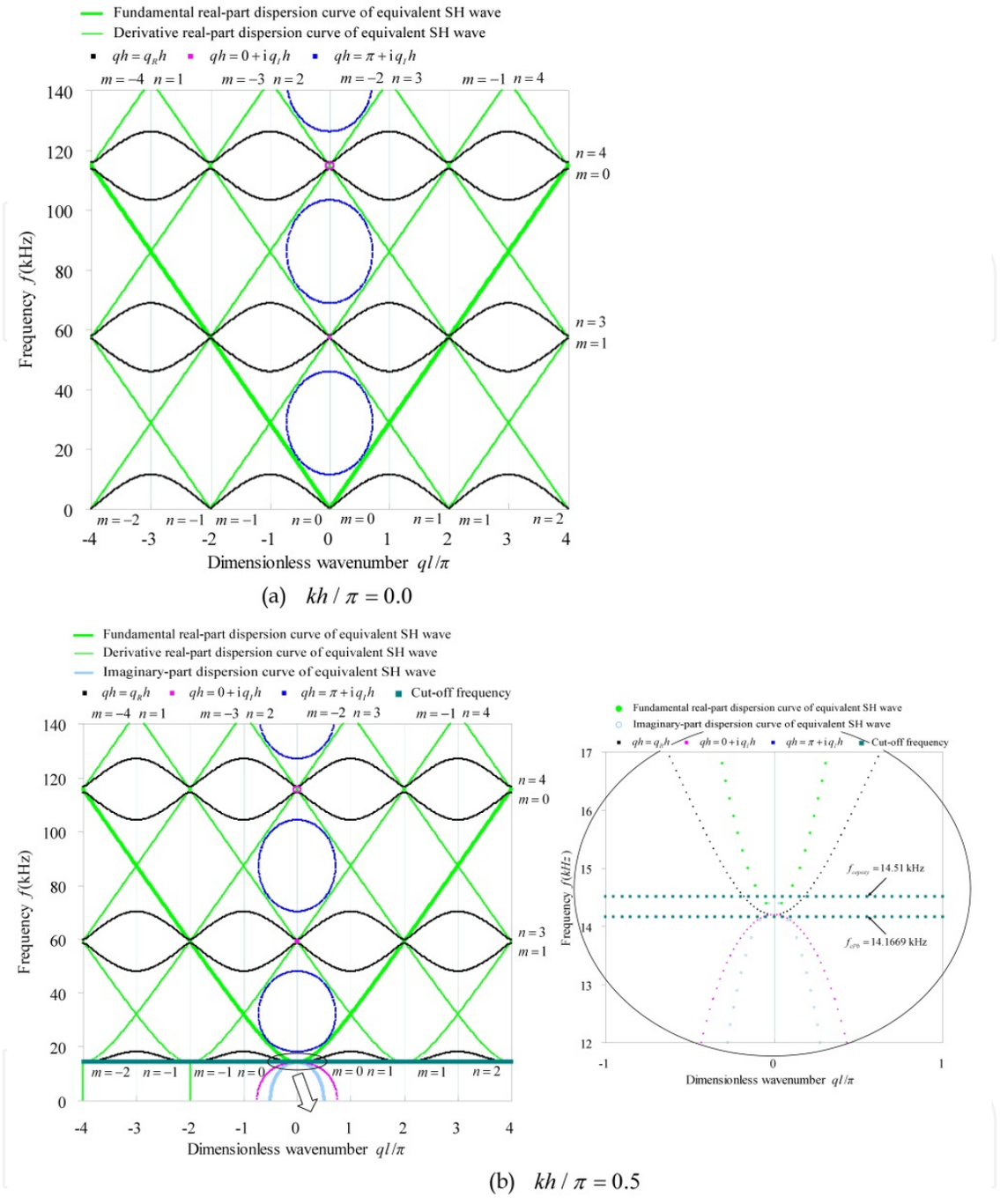

Figure 4. The band structures of characteristic SH waves and the dispersion curves of equivalent SH waves below 140 kHz in the periodic ternary layered medium consisting of one Pb layer and two epoxy layers

It is clearly seen from Figs. (4a) and (4b) that above the maximum cutoff frequency $\omega_{c\max}$ ($\omega_{c\max} = 0 = \omega_{c\min}$ while $kh/\pi = 0.0$), the dispersion curves of the equivalent SH waves have only the real part. In this case the fundamental and derivative dispersion curves of equivalent SH waves serve as the baselines during the band-structure formation of characteristic SH waves. In the forming process of the band structures, the dispersion curves

first separate with respect to frequency at the intersections $\gamma_{se}h + 2m\pi = -\gamma_{se}h + 2n\pi = I\pi$ (I is an arbitrary integer) representing the boundaries of the Brillouin zone to give the stop-bands, in which the attenuation constant spectra with phase 0 and phase π corresponding to even numbers and odd numbers of I, respectively. The intermediate segments of dispersion curves between the adjacent intersections are disturbed to form the phase constant spectra in the pass-bands. Figure (4b) also shows below the minimum cutoff frequency $\omega_{c\min}$ as $kh/\pi \neq 0.0$, the dispersion curves of the equivalent SH waves have only the imaginary part. In this case the dispersion curve serve as the baseline during the formation of the attenuation constant spectrum in the first stop-band, which is emerged due to the cutoff property of the SH waves in the constituent layers.

It should be emphasized that although the above example is a simple periodic ternary layered structure, the obtained property and formation of SH wave band structures are in fact also applicable to SH waves in all periodic layered isotropic media.

3. Analysis of acoustic waves in integrated multi-layered structures

Various multi-layered acoustic wave devices with Bragg Cell can be modeled by the multi-layered structures of infinite lateral extent depicted in Fig. 5, which including both non-piezoelectric layers and piezoelectric layers. Usually, the electrodes, support layers and substrate consist of elastic (non-piezoelectric) layers. The propagation media consist of

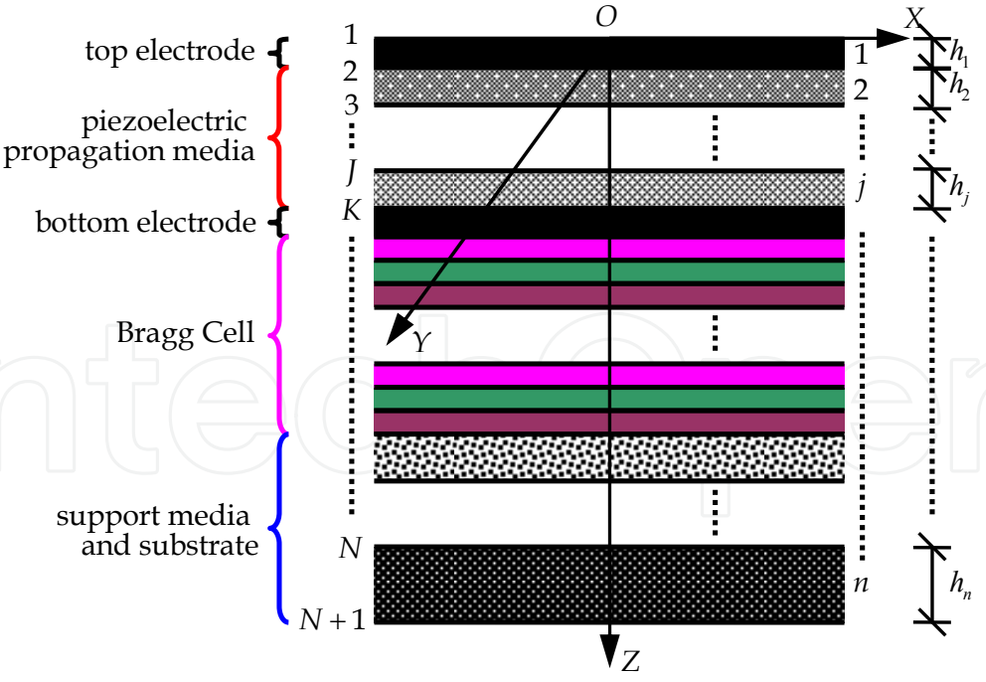

Figure 5. The schematic of multi-layered structures consisting of n layers for modeling the multi-layered acoustic wave devices

piezoelectric single-layer or multi-layers. The Bragg Cell can currently be made of alternate elastic layers such as W and SiO_2 or alternate elastic and piezoelectric layers such as SiO_2

and AlN (Lakin, 2005), and may in the future be made of alternate piezoelectric layers. Assume in the multi-layered model, each one of the n layers is homogeneous and the adjacent two layers are perfectly connected. To establish a general formulation for the analysis of various multi-layered acoustic wave devices with Bragg Cell, each layer in the multi-layered model is assumed as arbitrarily anisotropic. From up to down, the layers are denoted in order by numbers 1 to n, and the top surface, interfaces and bottom surface in turn are denoted by numbers 1 to $N+1$ ($N=n$). Thus, the upper and lower bounding faces of an arbitrary layer j ($j=1,2,\cdots,n$) are denoted by J ($J=j$) and K ($K=j+1$), respectively, and the layer j will also be referred to as JK or KJ. Moreover, a global coordinate system (X,Y,Z) with its origin located on the top surface and the Z-axis along the thickness direction, as shown in Fig. 5, is utilized to describe the integrated multi-layered structure.

3.1. Modeling of the non-piezoelectric layers (electrode, Bragg Cell, support layer and substrate)

Based on the three-dimensional linear elasticity (Stroh, 1962), the equations governing the dynamic state of a homogeneous, arbitrarily anisotropic elastic medium in absence of body forces can be written as

$$\sigma_{ij} = c_{ijkl}(u_{k,l} + u_{l,k})/2, \quad \sigma_{ij,j} = \rho\ddot{u}_i \tag{27}$$

where the comma in the subscripts and the dot above the variables imply spatial and time derivatives, σ_{ij} and u_i are respectively the stress and the displacement tensors, c_{ijkl} denotes the elastic constant tensor having at most 21 independent components, and ρ is the material density.

In the case of layer configuration, the state space formalism (Tarn, 2002a) can be adopted to describe mathematically the dynamic state of the medium. Referring to the global coordinate system (X,Y,Z) in Fig. 5, we divide the stresses into two groups: the first consists of the components on the plane of $Z=\text{constant}$, and the second consists of the remaining components. The combination of the displacement vector $\mathbf{v}_u=[u,v,w]^{\mathrm{T}}$ and the vector of first group stresses $\mathbf{v}_\sigma=[\tau_{zx},\tau_{zy},\sigma_z]^{\mathrm{T}}$ gives the state vector $\mathbf{v}=[(\mathbf{v}_u)^{\mathrm{T}},(\mathbf{v}_\sigma)^{\mathrm{T}}]^{\mathrm{T}}$.

3.2. Modeling of the piezoelectric layers (propagation media and Bragg Cell)

According to the three-dimensional linear theory of piezoelectricity (Ding & Chen, 2001), the dynamic governing equations for the arbitrarily anisotropic piezoelectric medium in absence of both body forces and free charges are

$$\begin{cases} \sigma_{ij} = c_{ijkl}(u_{k,l} + u_{l,k})/2 + e_{kij}\varphi_{,k} \\ D_i = e_{ikl}(u_{k,l} + u_{l,k})/2 - \beta_{ik}\varphi_{,k} \end{cases}, \begin{cases} \sigma_{ij,j} = \rho\ddot{u}_i \\ D_{i,i} = 0 \end{cases} \tag{28}$$

where D_i and φ are respectively the electric displacement and the electric potential tensors, e_{kij} and β_{ik} are the piezoelectric and the permittivity constant tensors having at most 18 and 6 independent components, respectively, and all the remaining symbols have the same meanings as the corresponding ones in Eq. (27). It is seen from Eq. (28) that the coupling between the mechanical and electrical fields is considered.

Similar to the arbitrarily anisotropic elastic layer, an arbitrarily anisotropic piezoelectric layer can also be described mathematically by the state space formalism (Tarn, 2002b). In view of the global coordinate system (X,Y,Z) in Fig. 5, the state vector is also represented as $\mathbf{v}=[(\mathbf{v}_u)^{\mathrm{T}},(\mathbf{v}_\sigma)^{\mathrm{T}}]^{\mathrm{T}}$, but with $\mathbf{v}_u=[u,v,w,\varphi]^{\mathrm{T}}$ being the generalized displacement vector and $\mathbf{v}_\sigma=[\tau_{zx},\tau_{zy},\sigma_z,D_z]^{\mathrm{T}}$ the generalized stress vector of the first group.

3.3. The state equations and solutions of non-piezoelectric and piezoelectric layers

By virtue of the triple Fourier transform pairs as follows

$$\begin{aligned}\hat{f}(k_x,k_y;z;\omega)&=\int_{-\infty}^{+\infty}\mathrm{e}^{-\mathrm{i}\omega t}\,\mathrm{d}\,t\int_{-\infty}^{+\infty}\int_{-\infty}^{+\infty}f(x,y,z,t)\mathrm{e}^{(\mathrm{i}k_x x+\mathrm{i}k_y y)}\,\mathrm{d}\,x\,\mathrm{d}\,y,\\ f(x,y,z,t)&=\int_{-\infty}^{+\infty}\frac{1}{2\pi}\mathrm{e}^{\mathrm{i}\omega t}\,\mathrm{d}\,\omega\int_{-\infty}^{+\infty}\int_{-\infty}^{+\infty}(\frac{1}{2\pi})^2\,\hat{f}(k_x,k_y;z;\omega)\mathrm{e}^{-(\mathrm{i}k_x x+\mathrm{i}k_y y)}\,\mathrm{d}\,k_x\,\mathrm{d}\,k_y\end{aligned} \tag{29}$$

the dynamic governing equations (27) and (28) in the time-space domain can be transformed into those in the frequency-wavenumber domain. The quantity ω can be interpreted as the circular frequency, k_x and k_y are interpreted as the wavenumbers in the x and y directions, respectively. $\mathrm{i}=\sqrt{-1}$ is the unit imaginary. The z-dependent variable in the frequency-wavenumber domain is indicated by an over caret. Adopting the state space formalism (Tarn, 2002a, 2002b), we can reduce the transformed dynamic governing equations of a material layer corresponding to Eqs. (27) and (28) in right-handed coordinate systems, by eliminating the second group of generalized stresses, to the state equation as follows

$$\frac{\mathrm{d}\,\hat{\mathbf{v}}(z)}{\mathrm{d}\,z}=\mathbf{A}\hat{\mathbf{v}}(z) \tag{30}$$

It is noted that the transformed state vector $\hat{\mathbf{v}}(z)$ contains $n_v/2$ generalized displacement components and $n_v/2$ generalized stress components, with $n_v=6$ and $n_v=8$ for a non-piezoelectric (elastic) layer and a piezoelectric layer, respectively. Thus, the state equation is a system of n_v first-order ordinary differential equations. The $n_v\times n_v$ coefficient matrix $\mathbf{A}$ of the state equation can be written in a blocked form

$$\mathbf{A}=\begin{bmatrix}-\mathrm{i}\mathbf{G}_{33}^{-1}\mathbf{W} & \mathbf{G}_{33}^{-1}\\ -\rho\omega^2\mathbf{M}+k_x^2\mathbf{G}_{11}+k_y^2\mathbf{G}_{22}+k_xk_y\left(\mathbf{G}_{12}+\mathbf{G}_{21}\right)-\mathbf{W}^{\mathrm{T}}\mathbf{G}_{33}^{-1}\mathbf{W} & -\mathrm{i}\,\mathbf{W}^{\mathrm{T}}\mathbf{G}_{33}^{-1}\end{bmatrix} \tag{31}$$

where $\mathbf{W} = -(k_x \mathbf{G}_{31} + k_y \mathbf{G}_{32})$. Assuming that the correspondence between the digital and coordinate indices follows $1 \to x$, $2 \to y$ and $3 \to z$, we have

$$\mathbf{G}_{kl} = \begin{bmatrix} c_{1k1l} & c_{1k2l} & c_{1k3l} \\ c_{2k1l} & c_{2k2l} & c_{2k3l} \\ c_{3k1l} & c_{3k2l} & c_{3k3l} \end{bmatrix}, \ \mathbf{M} = \mathbf{I}_3 \tag{32}$$

for a layer of arbitrarily anisotropic elastic material, and

$$\mathbf{G}_{kl} = \begin{bmatrix} c_{1k1l} & c_{1k2l} & c_{1k3l} & e_{l1k} \\ c_{2k1l} & c_{2k2l} & c_{2k3l} & e_{l2k} \\ c_{3k1l} & c_{3k2l} & c_{3k3l} & e_{l3k} \\ e_{k1l} & e_{k2l} & e_{k3l} & -\beta_{kl} \end{bmatrix}, \mathbf{M} = \begin{bmatrix} \mathbf{I}_3 & 0 \\ 0 & 0 \end{bmatrix} \tag{33}$$

for a layer of arbitrarily anisotropic piezoelectric material, with $\mathbf{I}_3$ the identity matrix of order 3.

According to the theory of ordinary differential equation (Coddington & Levinson, 1955), the solution to the state equation (30) can be expressed, in a form of traveling waves, as

$$\begin{aligned} \hat{\mathbf{v}}(z) &= \mathbf{\Phi} \exp(\mathbf{\Lambda} z)\mathbf{w} = \begin{bmatrix} \mathbf{\Phi}_- & \mathbf{\Phi}_+ \end{bmatrix} \begin{bmatrix} \exp(\mathbf{\Lambda}_- z) & \mathbf{0} \\ \mathbf{0} & \exp(\mathbf{\Lambda}_+ z) \end{bmatrix} \begin{Bmatrix} \mathbf{a} \\ \mathbf{d} \end{Bmatrix} \\ &= \begin{Bmatrix} \hat{\mathbf{v}}_u(z) \\ \hat{\mathbf{v}}_\sigma(z) \end{Bmatrix} = \begin{Bmatrix} \mathbf{\Phi}_u \\ \mathbf{\Phi}_\sigma \end{Bmatrix} \exp(\mathbf{\Lambda} z)\mathbf{w} = \begin{bmatrix} \mathbf{\Phi}_{u-} & \mathbf{\Phi}_{u+} \\ \mathbf{\Phi}_{\sigma-} & \mathbf{\Phi}_{\sigma+} \end{bmatrix} \begin{bmatrix} \exp(\mathbf{\Lambda}_- z) & \mathbf{0} \\ \mathbf{0} & \exp(\mathbf{\Lambda}_+ z) \end{bmatrix} \begin{Bmatrix} \mathbf{a} \\ \mathbf{d} \end{Bmatrix}, \end{aligned} \tag{34}$$

where $\exp(\cdot)$ denotes the matrix exponential function, $\mathbf{\Lambda}$ and $\mathbf{\Phi}$ are respectively the $n_v \times n_v$ diagonal eigenvalue matrix and square eigenvector matrix of the coefficient matrix $\mathbf{A}$, $\mathbf{w}$ is the vector of undetermined wave amplitudes with n_v components. $\mathbf{\Lambda}_-$ ($n_a \times n_a$) and $\mathbf{\Lambda}_+$ ($n_d \times n_d$) are the diagonal sub-matrices of $\mathbf{\Lambda}$ corresponding respectively to the arriving wave vector $\mathbf{a}$ with n_a wave amplitudes and the departing wave vector $\mathbf{d}$ with n_d wave amplitudes. $\mathbf{\Phi}_-$ ($n_v \times n_a$) and $\mathbf{\Phi}_+$ ($n_v \times n_d$) are the corresponding sub matrices of $\mathbf{\Phi}$. $\mathbf{\Phi}_u$ and $\mathbf{\Phi}_\sigma$ are the $n_v/2 \times n_v$ sub-matrices of $\mathbf{\Phi}$ corresponding to the generalized displacement and stress vectors, respectively. The sub-matrices $\mathbf{\Phi}_{u-}$, $\mathbf{\Phi}_{\sigma-}$, $\mathbf{\Phi}_{u+}$ and $\mathbf{\Phi}_{\sigma+}$ are defined accordingly. It should be noted that $\mathbf{a}$ consists of those wave amplitudes w_i in $\mathbf{w}$, which correspond to the eigenvalues λ_i satisfying $\mathrm{Re}(-\lambda_i) < 0$ or $\mathrm{Re}(-\lambda_i) = 0, \mathrm{Im}(-\lambda_i) < 0$, and the remaining wave amplitudes in $\mathbf{w}$ form $\mathbf{d}$. Obviously, we always have $\mathbf{w} = [\mathbf{a}^{\mathrm{T}}, \mathbf{d}^{\mathrm{T}}]^{\mathrm{T}}$ and $n_a + n_d = n_v$.

3.4. Reverberation-ray matrix analysis of integrated multi-layered structures

3.4.1. Description of the structural system

Within the framework of MRRM, the physical variables associated with any surface/interface J ($J=1,2,\cdots,N+1$) will be described in the global coordinate system (X,Y,Z) as shown in Fig. 5 for the convenience of system analysis, and will be affixed with single superscript J to indicate their affiliation. The physical variables associated with any layer j (i.e. JK or KJ, $j=1,2,\cdots,n$) will be described in the local dual coordinates (x^{JK},y^{JK},z^{JK}) or (x^{KJ},y^{KJ},z^{KJ}) as shown in Fig. 6 for the sake of member analysis, and will be affixed with double superscripts JK or KJ to denote the corresponding coordinate system and the pertaining layer. To make the sign convection clear, physical variables are deemed to be positive as it is along the positive direction of the pertinent coordinate axis.

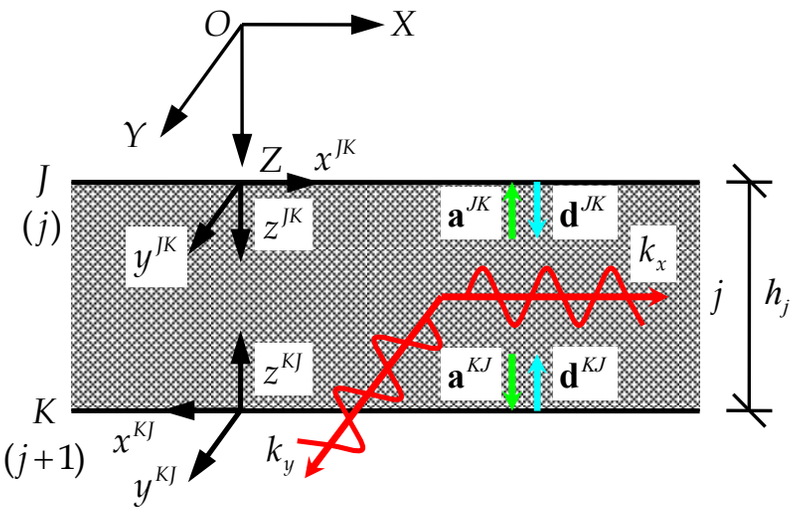

Figure 6. Description of a typical layer j within the multi-layered model in local dual coordinates

3.4.2. Traveling wave solutions to the state variables

It is seen from Fig. 6 that the local dual coordinates are both right-handed, thus the state equations for an arbitrary layer j (i.e. JK or KJ) in (x^{JK},y^{JK},z^{JK}) and (x^{KJ},y^{KJ},z^{KJ}) have the same form as Eq. (30). The traveling wave solutions to them can be written according to Eq. (34) as follows

$$\begin{Bmatrix}\hat{\mathbf{v}}_u^{JK}(z^{JK})\\ \hat{\mathbf{v}}_\sigma^{JK}(z^{JK})\end{Bmatrix}=\begin{Bmatrix}\mathbf{\Phi}_u^{JK}\\ \mathbf{\Phi}_\sigma^{JK}\end{Bmatrix}\exp(\mathbf{\Lambda}^{JK}z^{JK})\mathbf{w}^{JK}=\begin{bmatrix}\mathbf{\Phi}_{u-}^{JK} & \mathbf{\Phi}_{u+}^{JK}\\ \mathbf{\Phi}_{\sigma-}^{JK} & \mathbf{\Phi}_{\sigma+}^{JK}\end{bmatrix}\begin{bmatrix}\exp(\mathbf{\Lambda}_-^{JK}z^{JK}) & \mathbf{0}\\ \mathbf{0} & \exp(\mathbf{\Lambda}_+^{JK}z^{JK})\end{bmatrix}\begin{Bmatrix}\mathbf{a}^{JK}\\ \mathbf{d}^{JK}\end{Bmatrix}, \quad (35)$$

$$\begin{Bmatrix}\hat{\mathbf{v}}_u^{KJ}(z^{KJ})\\ \hat{\mathbf{v}}_\sigma^{KJ}(z^{KJ})\end{Bmatrix}=\begin{Bmatrix}\mathbf{\Phi}_u^{KJ}\\ \mathbf{\Phi}_\sigma^{KJ}\end{Bmatrix}\exp(\mathbf{\Lambda}^{KJ}z^{KJ})\mathbf{w}^{KJ}=\begin{bmatrix}\mathbf{\Phi}_{u-}^{KJ} & \mathbf{\Phi}_{u+}^{KJ}\\ \mathbf{\Phi}_{\sigma-}^{KJ} & \mathbf{\Phi}_{\sigma+}^{KJ}\end{bmatrix}\begin{bmatrix}\exp(\mathbf{\Lambda}_-^{KJ}z^{KJ}) & \mathbf{0}\\ \mathbf{0} & \exp(\mathbf{\Lambda}_+^{KJ}z^{KJ})\end{bmatrix}\begin{Bmatrix}\mathbf{a}^{KJ}\\ \mathbf{d}^{KJ}\end{Bmatrix}. \quad (36)$$

3.4.3. Scattering relations from coupling conditions on surfaces and at interfaces

Consider the compatibility of generalized displacements and the equilibrium of generalized stresses on surfaces and at interfaces. The spectral coupling equations on the top surface 1, at any interface J and on the bottom surface $N+1$ are expressed respectively as

$$\hat{\mathbf{v}}_u^{12}(0)=\hat{\mathbf{v}}_{uE}^{1},\quad \hat{\mathbf{v}}_\sigma^{12}(0)+\hat{\mathbf{v}}_{\sigma E}^{1}=\mathbf{0} \tag{37}$$

$$\mathbf{T}_u\hat{\mathbf{v}}_u^{JI}(0)=\hat{\mathbf{v}}_u^{JK}(0)=\hat{\mathbf{v}}_{uE}^{J},\quad \mathbf{T}_\sigma\hat{\mathbf{v}}_\sigma^{JI}(0)+\hat{\mathbf{v}}_\sigma^{JK}(0)+\hat{\mathbf{v}}_{\sigma E}^{J}=\mathbf{0} \tag{38}$$

$$\mathbf{T}_u\hat{\mathbf{v}}_u^{(N+1)N}(0)=\hat{\mathbf{v}}_{uE}^{(N+1)},\quad \mathbf{T}_\sigma\hat{\mathbf{v}}_\sigma^{(N+1)N}(0)+\hat{\mathbf{v}}_{\sigma E}^{(N+1)}=\mathbf{0} \tag{39}$$

where $\hat{\mathbf{v}}_{uE}^{1}$, $\hat{\mathbf{v}}_{uE}^{J}$ and $\hat{\mathbf{v}}_{uE}^{(N+1)}$ are the generalized displacement vectors of top surface 1, interface J and bottom surface $N+1$, respectively, $\hat{\mathbf{v}}_{\sigma E}^{1}$, $\hat{\mathbf{v}}_{\sigma E}^{J}$ and $\hat{\mathbf{v}}_{\sigma E}^{(N+1)}$ are the corresponding generalized stress vectors, $\mathbf{T}_u=\mathbf{T}_\sigma$ are the coordinate transformation matrix that equal to $<-1,1,-1>$ for non-piezoelectric (elastic) layers and $<-1,1,-1,-1>$ for piezoelectric layers. Here and after $<\cdot>$ denotes the (block) diagonal matrix with elements (or sub-matrices) only on the main diagonal.

It should be noticed that halves of all the components in vectors $\hat{\mathbf{v}}_{uE}^{1}$ and $\hat{\mathbf{v}}_{\sigma E}^{1}$, in vectors $\hat{\mathbf{v}}_{uE}^{J}$ and $\hat{\mathbf{v}}_{\sigma E}^{J}$, and in vectors $\hat{\mathbf{v}}_{uE}^{(N+1)}$ and $\hat{\mathbf{v}}_{\sigma E}^{(N+1)}$ are known, which are denoted by vectors $\hat{\mathbf{v}}_{K}^{1}$, $\hat{\mathbf{v}}_{K}^{J}$ and $\hat{\mathbf{v}}_{K}^{(N+1)}$, respectively. Substituting the solutions to the state variables of layers as given in Eqs. (35) and (36) into those coupling equations containing $\hat{\mathbf{v}}_{K}^{1}$, $\hat{\mathbf{v}}_{K}^{J}$ and $\hat{\mathbf{v}}_{K}^{(N+1)}$, we can obtain respectively the local scattering relations of top surface 1, interface J and bottom surface $N+1$ as follows

$$\mathbf{A}^1\mathbf{a}^1+\mathbf{D}^1\mathbf{d}^1=\mathbf{T}_K^1\hat{\mathbf{v}}_K^1=\mathbf{s}_0^1 \tag{40}$$

$$\mathbf{A}^J\mathbf{a}^J+\mathbf{D}^J\mathbf{d}^J=\mathbf{T}_K^J\hat{\mathbf{v}}_K^J=\mathbf{s}_0^J \tag{41}$$

$$\mathbf{A}^{N+1}\mathbf{a}^{N+1}+\mathbf{D}^{N+1}\mathbf{d}^{N+1}=\mathbf{T}_K^{N+1}\hat{\mathbf{v}}_K^{N+1}=\mathbf{s}_0^{N+1} \tag{42}$$

where $\mathbf{a}^1=\mathbf{a}^{12}$ ($\mathbf{d}^1=\mathbf{d}^{12}$), $\mathbf{a}^J=[(\mathbf{a}^{JI})^{\mathrm{T}},(\mathbf{a}^{JK})^{\mathrm{T}}]^{\mathrm{T}}$ ($\mathbf{d}^J=[(\mathbf{d}^{JI})^{\mathrm{T}},(\mathbf{d}^{JK})^{\mathrm{T}}]^{\mathrm{T}}$) and $\mathbf{a}^{N+1}=\mathbf{a}^{(N+1)N}$ ($\mathbf{d}^{N+1}=\mathbf{d}^{(N+1)N}$) are the arriving (departing) wave vectors of top surface 1, interface J and bottom surface $N+1$, respectively, the corresponding coefficient matrices $\mathbf{A}^1$ ($\mathbf{D}^1$), $\mathbf{A}^J$ ($\mathbf{D}^J$) and $\mathbf{A}^{N+1}$ ($\mathbf{D}^{N+1}$) have components extracted, in accordance with $\hat{\mathbf{v}}_{K}^{1}$, $\hat{\mathbf{v}}_{K}^{J}$ and $\hat{\mathbf{v}}_{K}^{(N+1)}$, from respectively $\mathbf{\Phi}_-^{12}$ ($\mathbf{\Phi}_+^{12}$), $[\mathbf{T}_v\mathbf{\Phi}_-^{JI},\mathbf{\Phi}_-^{JK}]$ ($[\mathbf{T}_v\mathbf{\Phi}_+^{JI},\mathbf{\Phi}_+^{JK}]$) and $\mathbf{T}_v\mathbf{\Phi}_-^{(N+1)N}$ ($\mathbf{T}_v\mathbf{\Phi}_+^{(N+1)N}$), $\mathbf{s}_0^1$, $\mathbf{s}_0^J$ and $\mathbf{s}_0^{(N+1)}$ are the excitation source vectors of top surface 1, interface J and bottom

surface $N+1$, respectively, the corresponding coefficient matrices $\mathbf{T}_K^1$, $\mathbf{T}_K^J$ and $\mathbf{T}_K^{N+1}$ consist of the components from $\mathbf{T}_v =< \mathbf{T}_u, \mathbf{T}_\sigma >$ in accordance with $\hat{\mathbf{v}}_K^1$, $\hat{\mathbf{v}}_K^J$ and $\hat{\mathbf{v}}_K^{(N+1)}$.

The local scattering relations of top surface, interfaces and bottom surface are grouped together from up to down to give the global scattering relation

$$\mathbf{A}\mathbf{a} + \mathbf{D}\mathbf{d} = \mathbf{s}_0, \tag{43}$$

where the global arriving and departing wave vectors $\mathbf{a}$ and $\mathbf{d}$ are

$$\begin{aligned} \mathbf{a} &= \left[(\mathbf{a}^{12})^{\mathrm{T}}, (\mathbf{a}^{21})^{\mathrm{T}}, (\mathbf{a}^{23})^{\mathrm{T}}, \cdots, (\mathbf{a}^{JI})^{\mathrm{T}}, (\mathbf{a}^{JK})^{\mathrm{T}}, \cdots, (\mathbf{a}^{N(N+1)})^{\mathrm{T}}, (\mathbf{a}^{(N+1)N})^{\mathrm{T}} \right]^{\mathrm{T}}, \\ \mathbf{d} &= \left[(\mathbf{d}^{12})^{\mathrm{T}}, (\mathbf{d}^{21})^{\mathrm{T}}, (\mathbf{d}^{23})^{\mathrm{T}}, \cdots, (\mathbf{d}^{JI})^{\mathrm{T}}, (\mathbf{d}^{JK})^{\mathrm{T}}, \cdots, (\mathbf{d}^{N(N+1)})^{\mathrm{T}}, (\mathbf{d}^{(N+1)N})^{\mathrm{T}} \right]^{\mathrm{T}} \end{aligned} \tag{44}$$

the corresponding coefficient matrices $\mathbf{A}$ and $\mathbf{D}$ are

$$\mathbf{A} =< \mathbf{A}^1, \mathbf{A}^2, \cdots, \mathbf{A}^J, \cdots, \mathbf{A}^{N+1} >, \quad \mathbf{D} =< \mathbf{D}^1, \mathbf{D}^2, \cdots, \mathbf{D}^J, \cdots, \mathbf{D}^{N+1} > \tag{45}$$

and $\mathbf{s}_0 = \left[(\mathbf{s}_0^1)^{\mathrm{T}}, (\mathbf{s}_0^2)^{\mathrm{T}}, \cdots, (\mathbf{s}_0^J)^{\mathrm{T}}, \cdots, (\mathbf{s}_0^{(N+1)})^{\mathrm{T}} \right]^{\mathrm{T}}$ is the global excitation source vector.

It is noticed that the exponential functions in the solutions to the state variables of layers as shown in Eqs. (35) and (36) disappear in the scattering relations, since the thickness coordinates on the surfaces and at the interfaces are always zero in the corresponding local coordinates. This is the main advantage of introducing the local dual coordinates.

3.4.4. Phase relations from compatibility conditions of layers

Considering the compatibility between generalized displacements (generalized stresses) represented in local coordinates (x^{JK}, y^{JK}, z^{JK}) and the corresponding ones represented in (x^{KJ}, y^{KJ}, z^{KJ}) of any layer j (i.e. JK or KJ), we have

$$\hat{\mathbf{v}}_u^{JK}(z^{JK}) = \mathbf{T}_u \hat{\mathbf{v}}_u^{KJ}(h^{JK} - z^{KJ}), \ \hat{\mathbf{v}}_\sigma^{JK}(z^{JK}) = -\mathbf{T}_\sigma \hat{\mathbf{v}}_\sigma^{KJ}(h^{JK} - z^{KJ}) \tag{46}$$

where h^{JK} $(= h^{KJ})$ denotes the thickness of layer JK (KJ). Substitution of Eqs. (35) and (36) into Eq. (46), one obtains, by noticing $\mathbf{\Lambda}^{JK} = -\mathbf{\Lambda}^{KJ}$, $\mathbf{\Phi}^{JK} = \mathbf{T}_v \mathbf{\Phi}^{KJ}$, $\mathbf{T}_v = \mathbf{T}_v^{-1}$, $n_a^{JK} = n_d^{KJ}$ and $n_d^{JK} = n_a^{KJ}$, the local phase relation of a typical layer j (i.e. JK or KJ)

$$\begin{Bmatrix} \mathbf{a}^{JK} \\ \mathbf{a}^{KJ} \end{Bmatrix} = \begin{bmatrix} \exp(-\mathbf{\Lambda}_-^{JK} h^{JK}) & \mathbf{0} \\ \mathbf{0} & \exp(\mathbf{\Lambda}_+^{JK} h^{JK}) \end{bmatrix} \begin{Bmatrix} \mathbf{d}^{KJ} \\ \mathbf{d}^{JK} \end{Bmatrix} = \begin{bmatrix} \mathbf{P}^{JK} & \mathbf{0} \\ \mathbf{0} & \mathbf{P}^{KJ} \end{bmatrix} \begin{bmatrix} \mathbf{0} & \mathbf{I}_a^{JK} \\ \mathbf{I}_d^{JK} & \mathbf{0} \end{bmatrix} \begin{Bmatrix} \mathbf{d}^{JK} \\ \mathbf{d}^{KJ} \end{Bmatrix} \tag{47}$$

where $\mathbf{P}^{JK} = \exp(-\mathbf{\Lambda}_{-}^{JK} h^{JK})$ and $\mathbf{P}^{KJ} = \exp(\mathbf{\Lambda}_{+}^{JK} h^{JK})$ are respectively the $n_a^{JK} \times n_a^{JK}$ and $n_d^{JK} \times n_d^{JK}$ diagonal local phase matrices, and $\mathbf{I}_a^{JK}$ and $\mathbf{I}_d^{JK}$ are identity matrices of order n_a^{JK} and n_d^{JK}, respectively.

Grouping together the local phase relations for all layers from up to down, one obtains the global phase relation

$$\mathbf{a} = \mathbf{PUd} \tag{48}$$

where $\mathbf{P}$ and $\mathbf{U}$ are respectively the blocked diagonal global phase matrix and global permutation matrix composed of

$$\mathbf{P} = < \mathbf{P}^{12}, \mathbf{P}^{21}, \mathbf{P}^{23}, \cdots, \mathbf{P}^{JI}, \mathbf{P}^{JK}, \cdots, \mathbf{P}^{N(N+1)}, \mathbf{P}^{(N+1)N} > \tag{49}$$

$$\mathbf{U} = < \mathbf{U}^{12}, \mathbf{U}^{23}, \cdots, \mathbf{U}^{JK}, \cdots, \mathbf{U}^{N(N+1)} >, \quad \mathbf{U}_{n_v \times n_v}^{JK} = \begin{bmatrix} \mathbf{0} & \mathbf{I}_a^{JK} \\ \mathbf{I}_d^{JK} & \mathbf{0} \end{bmatrix} \tag{50}$$

3.4.5. System equation and dispersion equation

The global scattering relation in Eq. (43) and the global phase relation in Eq. (48) both contain $n_v \times N$ equations for the $n_v \times N$ unknown arriving wave amplitudes (in $\mathbf{a}$) and $n_v \times N$ unknown departing wave amplitudes (in $\mathbf{d}$). Thus the wave vectors $\mathbf{a}$ and $\mathbf{d}$ can be determined accordingly. Substitution of Eq. (48) into Eq. (43) gives the system equation

$$(\mathbf{APU} + \mathbf{D})\mathbf{d} = \mathbf{Rd} = \mathbf{s}_0 \tag{51}$$

where $\mathbf{R} = \mathbf{APU} + \mathbf{D}$ is the system matrix.

If there is no excitation ($\mathbf{s}_0 = \mathbf{0}$), i.e. the free wave propagation problem is considered, the vanishing of the system matrix determinant yields the following dispersion equation

$$\left| \mathbf{R}(k_x, k_y; \omega) \right| = \mathbf{0} \tag{52}$$

which may be solved numerically by a proper root searching technique (Guo, 2008). Thus, the complete propagation characteristics of various waves can be obtained. In particular, the resonant frequency of the multi-layered structures can be obtained as $k_x = k_y = 0$.

It should be noted that the above proposed formulation of MRRM (Guo & Chen, 2008a, 2008b; Guo, 2008; Guo et al., 2009) excludes any exponentially growing function and matrix inversion, therefore possesses unconditionally numerical stability and enables inclusion of surface and interface wave modes.

3.5. Numerical examples

In this section, the above proposed formulation of MRRM for analyzing the propagation characteristics of various waves in the integrated acoustic wave devices are validated by a bulk acoustic resonator (BAR) consisting of 0.3μm Al film as the top electrode, 3.0μm AlN film as the propagation medium, 0.3μm Al film as the bottom electrode, alternate 0.81μm SiO_2 and 1.76μm AlN layers as the Bragg Cell, 0.81μm SiO_2 layer as the support medium and 42.6μm Si layer as the substrate. The material parameters of the exemplified BAR used in the calculation are given in Table 1.

Type of material	Material	Material parameters			
		Elastic constants (GPa)	Mass density (kg/m^3)	Dielectric constant ($\times 8.854 \times 10^{-12}$ F/m)	Piezoelectric constants (C/m^2)
Isotropic elastic material	Al	$E = 69$, $G = 26$	$\rho = 2700$	$\varepsilon = 1.6$	—
	SiO_2	$E = 70$, $G = 29.915$	$\rho = 2200$	$\varepsilon = 3.9$	—
Transversely isotropic elastic material	Si	$c_{11} = c_{22} = c_{33} = 164.8$, $c_{12} = c_{13} = c_{23} = 63.5$, $c_{44} = c_{55} = 79$, $c_{66} = 50.65$	$\rho = 2330$	$\varepsilon_{11} = \varepsilon_{22} = \varepsilon_{33} = 11.8$	—
Transversely isotropic piezoelectric material	AlN	$c_{11} = c_{22} = 345$, $c_{33} = 395$, $c_{12} = 125$, $c_{13} = c_{23} = 120$, $c_{44} = c_{55} = 118$, $c_{66} = 110$	$\rho = 3512$	$\varepsilon_{11} = \varepsilon_{22} = 9$, $\varepsilon_{33} = 11$	$e_{15} = e_{24} = -0.48$, $e_{31} = e_{32} = -0.58$, $e_{33} = 1.55$

Table 1. Material properties of the exemplified bulk acoustic resonator

The resonant frequencies, represented by the engineering frequency $f = \omega / 2\pi$ for the convenience of engineering application, of various waves in the multi-layered BAR are calculated by the formulation presented in Section 3.4 as the wavenumbers k_x and k_y are set to be zero. In order to show the influence of the number of unit cells in the Bragg Cell on the wave characteristics, Bragg Cells with 2 and 5 unit cells are respectively considered. Moreover, for sake of exploring the effects of electrodes, Bragg Cell and substrate on the wave characteristics in the propagation medium, the resonant frequencies of the 3.0μm AlN film, 3.0μm AlN film with top and bottom electrodes, and the bulk acoustic resonator without substrate and with 5 unit cells in the Bragg Cell are also calculated. The obtained first fifteen resonant frequencies of these multi-layered structures are listed and compared in Table 2.

Order	3.0μm AlN film	3.0μm AlN film with electrodes	The whole BAR with 2 unit cells in the Bragg Cell	The whole BAR with 5 unit cells in the Bragg Cell	The whole BAR without substrate and with 5 unit cells in the Bragg Cell
1	0.9750	0.8380	0.0523	0.0441	0.1275
2	1.8217	2.2329	0.1038	0.0655	0.2517
3	1.9328	3.3316	0.1564	0.0885	0.3810
4	2.9014	4.8778	0.2096	0.1332	0.5130
5	3.6438	5.2997	0.2608	0.1755	0.6320
6	3.8643	5.7110	0.3106	0.2031	0.8749
7	4.8326	6.5112	0.3645	0.2206	1.0236
8	5.4657	8.9604	0.4771	0.2652	1.2409
9	5.7971	9.7544	0.5747	0.2668	1.3322
10	6.7639	10.5897	0.6334	0.3066	1.4596
11	7.2868	12.1454	0.6964	0.3350	1.7058
12	7.7296	13.2501	0.7610	0.3542	1.7985
13	8.6956	14.6379	0.8262	0.3984	1.9343
14	9.1095	15.4651	0.8727	0.4394	2.1422
15	9.6604	16.2959	0.8943	0.4679	2.2865

Table 2. Effects of components on the first fifteen frequencies of the exemplified BAR (GHz)

From Table 2, it is seen that all component layers in the multi-layered bulk acoustic wave device have obvious influence on the wave propagation characteristics, which validates the necessity to model the multi-layered acoustic wave devices by an integrated model with all components considered. The electrodes generally raise the resonant frequencies in the propagation medium except for the first mode. Adding unit cells of the Bragg Cell and the appending of substrate in the multilayered BAR will reduce the resonant frequencies and increase the number of wave modes in a given frequency range. These findings about the effects of electrodes, Bragg Cell and substrate on wave characteristics in the multilayered acoustic wave devices can be used in the design of these devices.

4. Conclusion

The accurate analysis and design of layered Bragg Cell and of multi-layered acoustic wave devices with Bragg Cell are studied by the method of reverberation-ray matrix in this chapter. We obtain the analysis formulation, the features and the formation of SH-wave band structures in layered Bragg Cell and the design rules of layered Bragg Cell according to SH-wave band requirements. A unified formulation of MRRM is attained for the analysis of multi-layered acoustic wave devices modeled by integrated multi-layers consisting of working media, electrodes, Bragg Cell, support layer and substrate. The effects of other components on the resonant characteristics in the working media are gained. All findings are validated by numerical examples. The study in this chapter leads to the following conclusions:

(1) In the SH-wave band structures of layered Bragg Cell, the phase constant spectra in pass-bands and the attenuation constant spectra in stop-bands occur alternately. The phase constant spectra of characteristic SH waves are formed from the dispersion curves of equivalent SH waves due to the zone folding effect and wave interference phenomenon. All the attenuation constant loops as $k = 0$ and the second and upper attenuation constant loops as $k \neq 0$ of characteristic SH waves are formed due to the separation of the dispersion curves of equivalent SH waves with respect to frequency during the forming of the phase spectra. The first attenuation constant loop as $k \neq 0$ of characteristic SH wave is formed due to the cutoff property of SH waves in constituent layers. The contrasts of SH-wave characteristic impedances of the constituent layers, the characteristic time of the unit cell and the characteristic times of the constituent layers are three kinds of essential parameters determining the formation of the band structures. The contrasts of SH-wave characteristic impedances decide whether the stop-bands due to periodicity of the periodic layered media exist or not. If yes, it further decides the widths of the frequency bands. The characteristic time of the unit cell decides how many pass-bands/stop-bands exist in a specified frequency range. The characteristic times of the constituent layers mainly decides the mid-frequencies of the frequency bands. These rules can be used for the design of the layered Bragg Cell according to SH-wave bands requirements.

(2) The proposed MRRM for integrated multi-layered acoustic wave devices is analytical based on distributed-parameter model, yields unified formulation, includes all wave modes and possesses unconditionally numerical stability. It therefore leads to high accurate results at small computational cost and is applicable to complex multilayered acoustic wave devices while combined with a uniform computer program.

(3) The integrated model considers nearly all the components in practical multi-layered acoustic wave devices, which definitely renders accurate wave propagation characteristics for guiding the proper design of and suppresses unfavorable spurious modes in the devices. Generally, the electrodes raise the resonant frequencies, while the Bragg Cell and the substrate reduce the resonant frequencies.

In summary, the MRRM, the understanding of SH wave bands in the Bragg Cell and the integrated modeling of multi-layered acoustic wave devices with Bragg Cell in this chapter will push forward the design of high-performed acoustic wave devices.

Author details

Yongqiang Guo
Key Laboratory of Mechanics on Disaster and Environment in Western China, Ministry of Education, and School of Civil Engineering and Mechanics, Lanzhou University, P.R.China

Weiqiu Chen
Department of Engineering Mechanics, Zhejiang University,P.R.China

Acknowledgement

This study was financially supported by the National Natural Science Foundation of China (Nos. 10902045 and 11090333), the Postdoctoral Science Foundation of China (Nos. 20090460155 and 201104019) and the Fundamental Research Funds for the Central Universities of China (Grant No. lzujbky-2011-9).

5. References

Adler, E.L. (2000). Bulk and surface acoustic waves in anisotropic solids, *International Journal of High Speed Electronics and Systems*, 10(3): 653-684.

Ballandras, S., Reinhardt, A., Laude, V., Soufyane, A., Camou, S., Daniau, W., Pastureaud, T., Steichen, W., Lardat, R., Solal, M. & Ventura, P. (2004) Simulations of surface acoustic wave devices built on stratified media using a mixed finite element/boundary integral formulation. *Journal of Applied Physics*, 96(12): 7731-7741.

Benetti, M., Cannata, D., Di Pietrantonio, F., Verona, E., Almaviva, S., Prestopino, G., Verona, C. & Verona-Rinati, G. (2008). Surface acoustic wave devices on AlN/single-crystal diamond for high frequency and high performances operation, *Proceedings of IEEE Ultrasonics Symposium, 1924-1927*, Beijing, China, Nov. 2008.

Benetti, M., Cannatta, D., Di Pietrantonio, F. & Verona, E. (2005). Growth of AlN piezoelectric film on diamond for high-frequency surface acoustic wave devices, *IEEE Transactions on Ultrasonics, Ferroelectrics, and Frequency Control*, 52: 1806–1811.

Brillouin, L. (1953). *Wave Propagation in Periodic Structures: Electric Filters and Crystal Lattices*, Dover Publications, New York.

Brizoual, L.L., Sarry, F., Elmazria, O., Alnot, P., Ballandras, S. & Pastureaud, T. (2008). GHz frequency ZnO/Si SAW device, *IEEE Transactions on Ultrasonics, Ferroelectrics, and Frequency Control*, 55(2): 442–450.

Chung, C.-J. Chen, Y.-C., Cheng, C.-C., Wang, C.-M. & Kao, K.-S. (2008). Superior dual mode resonances for 1/4λ solidly mounted resonators, *Proceedings of IEEE Ultrasonics Symposium, 250-253*, Beijing, China, Nov. 2008.

Coddington, E. A., Levinson, N. (1955). *Theory of Ordinary Differential Equations*, McGraw-Hill, New York.

Ding, H.J. & Chen, W.Q. (2001). *Three Dimensional Problems of Piezoelasticity*. Nova Science Publishers, New York.

Eringen, A.C. & Suhubi, E.S. (1975). *Elastodynamics II: Linear Theory*, Academic Press, New York.

Guo, Y.Q. & Chen, W.Q. (2010). Reverberation-ray matrix analysis of acoustic waves in multilayered anisotropic structures. *Acoustic Waves* (Edited by Don W. Dissanayake, ISBN: 978-953-307-111-4): 25-46.

Guo, Y.Q. & Chen, W.Q. (2008a). On free wave propagation in anisotropic layered media, *Acta Mechanica Solida Sinica*, 21: 500-506.

Guo, Y.Q. & Chen, W.Q. (2008b). Modeling of multilayered acoustic wave devices with the method of reverberation-ray matrix, *Symposium on Piezoelectricity, Acoustic Waves, and Device Applications* (SPAWDA 2008), 105-110.

Guo, Y.Q. (2008). *The Method of Reverberation-Ray Matrix and its Applications*, Doctorial dissertation. Zhejiang University, Hangzhou, China. (in Chinese)

Guo, Y.Q., Chen, W.Q. & Zhang, Y.L. (2009). Guided wave propagation in multilayered piezoelectric structures, *Science in China*, *Series G*: *Physics*, *Mechanics and Astronomy*, 52(7): 1094-1104.

Hashimoto, K., Omori, T. & Yamaguchi, M. (2009). Characterization of surface acoustic wave propagation in multi-layered structures using extended FEM/SDA software, *IEEE Transactions on Ultrasonics, Ferroelectrics, and Frequency Control*, 56(11): 2559–2564.

Hashimoto, K.Y. (2000). *Surface Acoustic Wave Devices in Telecommunications: Modeling and Simulation*, Springer, Berlin.

Kirsch, P., Assouar, M.B., Elmazria, O., Mortet, V., & Alnot, P. (2006). 5GHz surface acoustic wave devices based on aluminum nitride/diamond layered structure realized using electron beam lithography, *Applied Physics Letters*, 88: 223504.

Lakin, K.M. (2005). Thin film resonator technology, *IEEE Transactions on Ultrasonics, Ferroelectrics, and Frequency Control*, 52(5): 707-716.

Lowe, M.J.S. (1995). Matrix techniques for modeling ultrasonic waves in multilayered media, *IEEE Transactions on Ultrasonics, Ferroelectrics, and Frequency Control*, 42: 525-542.

Makkonen, T. (2005). *Numerical Simulations of Microacoustic Resonators and Filters*, Doctoral Dissertation. Helsinki University of Technology, Espoo, Finland.

Marechal, P., Haumesser, L., Tran-Huu-Hue, L.P., Holc, J., Kuscer, D., Lethiecq, M. & Feuillard, G. (2008). Modeling of a high frequency ultrasonic transducer using periodic structures, *Ultrasonics*, 48: 141–149.

Mead, D.J. (1996). Wave propagation in continuous periodic structures: Research contributions from Southampton, 1964–1995. *Journal of Sound and Vibration*, 190(3): 495–524.

Nakanishi, H., Nakamura, H., Hamaoka, Y., Kamiguchi, H. & Iwasaki, Y. (2008). Small-sized SAW duplexers with wide duplex gap on a SiO_2/Al/$LiNbO_3$ structure by using novel Rayleigh-mode spurious suppression technique, *Proceedings of IEEE Ultrasonics Symposium*, 1588-1591, Beijing, China, Nov. 2008.

Naumenko, N.F. (2010). A universal technique for analysis of acoustic waves in periodic grating sandwiched between multi-layered structures and its application to different types of waves, *Proceedings of IEEE Ultrasonics Symposium*, *1673-1676*, San Diego, USA, Oct. 2010.

Pao, Y.H., Chen, W.Q. & Su, X.Y. (2007). The reverberation-ray matrix and transfer matrix analyses of unidirectional wave motion, *Wave Motion*, 44: 419-438.

Pastureaud, T., Laude, V. & Ballandras, S. (2002). Stable scattering-matrix method for surface acoustic waves in piezoelectric multilayers, *Applied Physics Letters*, 80: 2544-2546.

Royer, D. & Dieulesaint, E. (2000). *Elastic Waves in Solids I: Free and Guided Propagation*, Springer, Berlin.

Shen, M.R. & Cao, W.W. (2000). Acoustic bandgap formation in a periodic structure with multilayer unit cells. *Journal of Physics D: Applied Physics*, 33: 1150–1154.

Stroh, A.N. (1962). Steady state problems in anisotropic elasticity, *Journal of Mathematics and Physics*, 41: 77-103.

Su, X.Y., Tian, J.Y. & Pao, Y.H. (2002). Application of the reverberation-ray matrix to the propagation of elastic waves in a layered solid, *International Journal of Solids and Structures*, 39: 5447-5463.

Tajic, A., Volatier, A., Aigner, R., Solal, M. (2010). Simulation of solidly mounted BAW resonators using FEM combined with BEM and/or PML, *Proceedings of IEEE Ultrasonics Symposium*, 181-184, San Diego, USA, Oct. 2010.

Tan, E.L. (2007). Matrix Algorithms for modeling acoustic waves in piezoelectric multilayers, *IEEE Transactions on Ultrasonics, Ferroelectrics, and Frequency Control*, 54: 2016-2023.

Tarn, J. Q. (2002a). A state space formalism for anisotropic elasticity. Part I: Rectilinear anisotropy, *International Journal of Solids and Structures*, 39: 5143-5155

Tarn, J. Q. (2002b). A state space formalism for piezothermoelasticity, *International Journal of Solids and Structures*, 39: 5173-5184

Wang, G., Yu, D.L., Wen, J.H., Liu, Y.Z., Wen, X.S. (2004). One-dimensional phononic crystals with locally resonant structures. *Physics Letters A*, 327: 512–521.

Wang, L. & Rokhlin, S.I. (2002). Recursive asymptotic stiffness matrix method for analysis of surface acoustic wave devices on layered piezoelectric media, *Applied Physics Letters*, 81: 4049-4051.

Wu, T.T. & Chen, Y.Y. (2002) Exact analysis of dispersive SAW devices on ZnO/diamond/Si-layered structures, *IEEE Transactions on Ultrasonics, Ferroelectrics, and Frequency Control*, 49: 142-149.

Yoon, G., & Park, J.-D. (2000). Fabrication of ZnO-based film bulk acoustic resonator devices using W/SiO_2 multilayer reflector, *IEEE Electronics Letters*, 36(16): 1435-1437.

Zhang, V.Y., Dubus, B., Lefebvre, J.E. & Gryba, T. (2008). Modeling of bulk acoustic wave devices built on piezoelectric stack structures: Impedance matrix analysis and network representation, *IEEE Transactions on Ultrasonics, Ferroelectrics, and Frequency Control*, 55(3): 704–716.

Zhang, V.Y., Lefebvre, J.E. & Gryba, T. (2006). Resonant transmission in stop bands of acoustic waves in periodic structures, *Ultrasonics*, 44(1): 899–904.